Deployment of Liner Systems in Extreme High Mud Weight Environments in Gas Wells

Abdullah H. Oqaili, Abdulaziz S. Alluhaydan, Peter C. Ezi, and Alvaro Tirado

ABSTRACT

During the development phase of a gas field, the abnormal pressure in a dolomitic limestone formation demanded an extremely high mud weight (MW) to control the well. The casing design of this case study field has entailed the installation of a 7" × 9⅝" liner hanger in combination with a liner top packer followed by a tie back to the surface. Due to this hole section being directly above the pay zone, it is crucial that the liner installation and the wellbore integrity are not compromised for the subsequent well completion.

The challenging downhole pressure conditions require a drilling MW up to 157 pcf (~ 21 ppg), where solids content could reach as high as 49% using conventional weighing materials. For a liner deployment, this means that the high concentration of solids can cause plugging in the setting ports of a conventional hydraulic liner hanger and running tool system, as well as causing high pressure to shear the gels on a complex mud rheology, increased equivalent circulating densities (ECDs) that can lead to fluid loss issues and problems of barite settling in the open hole, among others. Additionally, the thin balance between ECDs and the formation fracture pressures in this field generated numerous events of severe fluid loss during the liner deployment or while cementing. A liner not fully supported by cement — due to severe fluid loss during cementation — can experience ballooning, and be unable to withstand piston forces acting against the liner's top packer during well completion operations. These forces can, in some cases, exceed the ratings of the liner top packer's hold down slips, therefore allowing the packing element of the liner top packer to fail. An expensive workover operation may be necessary to decomplete and recomplete the well.

For these reasons, an optimized deployment strategy was planned and implemented to address these challenges. It included improvements to the hydraulic liner hanger and running tool system, calculations to simulate an optimal running speed of the liner, and enhanced procedures for liner deployment and cementation, including revised setting procedures for the liner hanger slips, and modifications to the drillpipe's wiper plug design.

The results of these improvements have reduced the failure rates of the liner equipment significantly, saving up to 30 days of nonproductive time (NPT) per well related to remedial jobs.

The objective of this article is to detail the benefits of implementation, detailed pre-job planning, improvements for optimal drilling mud properties and modifications to the liner hanger system, and procedures that resulted in successful deployments of liners in the field. In addition, a case study will be shared as a way to institute lessons learned and best practices.

INTRODUCTION

Field Background

To reach the reservoir section, a high-pressure zone must be drilled through and isolated by a cemented liner. Proper isolation from the pressurized formation is required because of the highly diverse pressure regimes between the reservoir section and high-pressure zone above it. The typical mud weight (MW) to drill through the high-pressure zone can reach up to 157 pcf (± 20.9 ppg), while the reservoir section requires a relatively lower mud density. Combining the two sections will result in exceeding the fracture pressure of the formation in the reservoir section.

The high-pressure zone is composed mainly of high salinity fluid — with chloride content higher than 100,000 ppm, which is trapped with streaks of anhydrates combined with dolomitic limestone. It is believed that the high pressurized zone was formed during tectonic and other geological events that happened in the past. The average length of the section is around 1,500 ft containing ±1,000 ft of high-pressure zone interval. In addition to being a high-pressure zone, it includes several intervals of weak formations that are naturally fractured. Most notably, this part of the formation has an extremely narrow MW window that can be as low as 1 pcf (0.15 ppg) in some places[1]. For this reason, managed pressure drilling (MPD) and cementing (MPC) techniques were used to manage this tight MW window and reach the liner point safely.

Mud Challenges

At the initial design, barite was used as the only weighting agent to build up the density of the mud. As mentioned earlier, the mud density required for this section can reach as high as

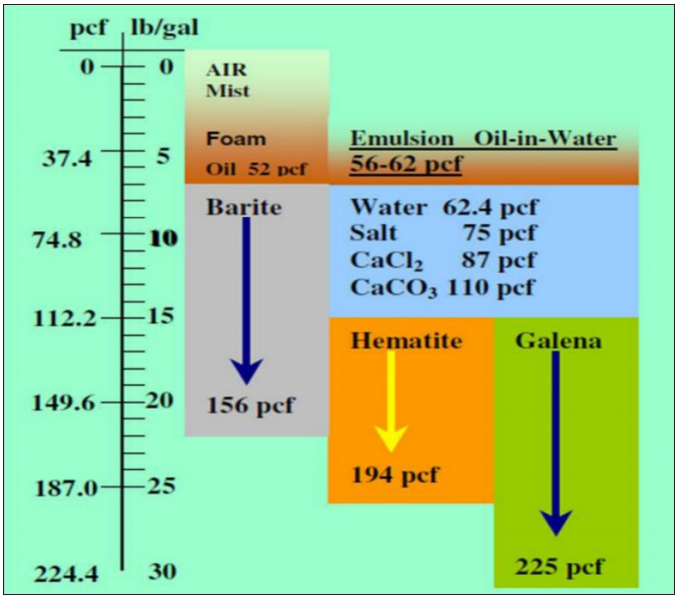

Fig. 1. MW range with different weighting agents[2].

157 pcf (~21 ppg). This means the barite system will be operated at its maximum limit of 156 pcf or 20.8 ppg, Fig. 1[2].

These drilling fluid conditions had their own challenges for hole instability, and subsequent effects on the liner deployment. For example, one of the issues of the barite system was barite settling — sagging. This condition occurs when barite particles settle downhole when circulation stops. It might cause the drillstring to plug or reduce the hydrostatic pressure, leading to a possible well control situation. To avoid the barite settlement, the rheology of the drilling fluid is increased to improve the suspension properties of the mud. Once the rheology increases, the equivalent circulating density (ECD) will increase, leading to possible loss circulation events. Drilling fluid losses to the formation while running the liner can lead to several problems. Mainly, the integrity of the cement cannot be guaranteed, due to loss of cement to the formation. Once the cement integrity is lost, it can lead to more complications such as what is called "wet shoe." This is a situation where there is no cement around the casing shoe; thereby compromising the well integrity. Remedial jobs are mandatory to fix the wet shoe, which is not always guaranteed, and it usually requires a high amount of nonproductive time (NPT). For these reasons, controlling the mud properties by decreasing the high rheology of the fluid is crucial to enable successful deployment of the liner system.

Liner Deployment

The abnormal mud density and solids content of the drilling mud used in the field were the main challenges to successfully deploy a conventional hydraulic liner hanger system. Due to the well instability conditions, the liner must have the ability to be circulated with no pressure restriction, rotated and reciprocated during running to mitigate the challenging wellbore conditions of the field, and at the same time provide an effective liner top and liner shoe isolation.

Cemented liners deployed under high solids content and high fluid losses are not very common, however, this field is an exception. As seen in Table 1, the approximate MW used to drill this section can reach up to 21 ppg. This requires a significant effort that includes detailed pre-job planning to identify and mitigate the challenges. Additionally, agreement between the execution and the planning teams is essential to implement the best practices and lessons learned to reduce the risk of failure, and select the equipment that is a best fit for the application.

Historically, under these mud conditions, conventional hydraulic liner hanger systems were not successful in achieving the objective of activating the hanger's slips. Due to the high solids content in the fluid, settling around the slips and clogging of the setting ports on the hydraulic activated tools are known as the main root cause in preventing the hanger slips to activate. Solids in the system also translate into a high shearing pressure for the running tool ball seat that in some cases can lead to fluid losses caused by the hammer effect against the formation. For these reasons, operators prefer mechanical liner hangers to be deployed in extreme high MW systems, however, if the liner must be rotated while working through tight spots, then a mechanical hanger becomes a limitation.

After the liner system is deployed and cemented, an isolation packer is activated above the liner hanger. To fully activate this packer, a sufficient force is required to be applied on it. This force is achieved by the bottom-hole assembly (BHA), which is used to run the system. In most of the vertical wells, transmitting the setting weight to the liner packer is not an issue due to the minimum drag in the well. In the S-shape wells in this field, it is more complicated to have an effective transfer of the set down weight to energize the slips of the tie back packers. Proper setting of the packer's slips is critical because after setting the packer, a negative test on top of the liner packer is required to confirm its integrity. This high drawdown pressure, reflecting the weight difference between the liner section MW and the completion fluid density, will exert a considerable force on the liner system, which can lead to excessive forces acting on the liner's top packer if the cementation was compromised by losses.

Location Type	City	MW (ppg)
Offshore	Belle Chasse	20
Land	Victoria	19.1
Offshore	Houma	18.7
Offshore	Great Yarmouth	20
Offshore	Kemaman	18.8
Offshore	Aberdeen	19.7
Land	Kuwait	20
Land	**Case study field**	**21**

Table 1. MW vs. fields around the world

UNDERSTANDING THE CHALLENGES

Hanger Setting Problems

The activation pressure of the hydraulic liner hanger and the running tool are the main limitations to circulating pressures during liner deployment. The simple solution to overcome this limit is to increase the standard setting pressures of the hanger and the running tool. Despite the adjustments, the pressure required to shear the high rheology of the drilling mud can still prematurely set the liner hanger. For that reason, a hydraulic liner hanger with a pressure balanced system was selected for this field, as this allows high-pressure circulation through the unstable well conditions and extreme high MW systems. The pressure balanced design is unaffected by circulating pressures, which prevents it from premature setting while circulating at high pressures if required.

Liner Top Packer Leaks

Total losses during cementing is an unfavorable condition that can have a severe impact on the integrity of the well. In the majority of cases of lost circulation, the liner top packer is set immediately after the cement job. This practice is done in this field mainly for well control purposes to have the well secured during tripping out with the running tool assembly. Afterward, a negative test is done on the liner packer in which two main effects exert force against the liner top packer. The piston force below the seal element is driven by the differential between the formation pressure and the fluid above the element, and the reverse ballooning force of the heavier fluid on the annulus.

These two forces push across the packer element and packer hold down system against the lighter fluid inside the liner. If the liner does not have the support of the cement as a result of the severe fluid loss situation, the combination of these forces — in some cases — can exceed the rating of the hold down slips of the liner top packer. This is illustrated in Fig. 2, where it shows the net forces that are acting on the liner packer/hanger assembly during negative testing of the liner system. If the hold down slips capability is not enough to provide an anchoring force to the packer element, the packer will fail.

Transferring the Weight to the Tie-Back Packer

Once it was confirmed that there was a leak through the liner top, a tie back packer is required to fix the leak.

Insufficient transfer of weight downhole through a deviated S-shape well was identified as the main root cause for not setting the liner top packer, and therefore, having a liner top leak. Table 2 shows the weight difference when transferring the weight to set the hold down slips at the packer depth on an S-shape well trajectory.

Cement Displacement

In one event, the liner wiper plug was found on top of the liner — not in the landing collar where it supposed to be — while performing the subsequent cement clean out trip. The result of the investigation concluded that the most likely explanation was that the displacement heavy mud bypassed the drillpipe dart due to the wide outside diameter (OD) of the fins, which

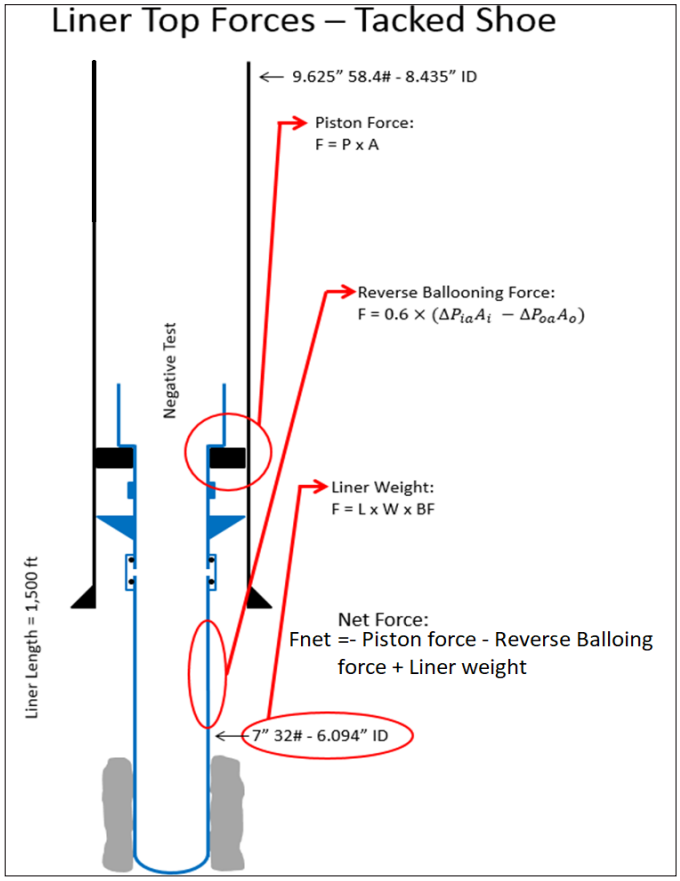

Fig. 2. Net forces on the liner in case of losses during the cement job.

Slack Off on Surface (Klb)	Weight on Packer (Klb)	Difference (Klb)
60	60	0
70	70	0
80	79.5	-0.5
90	84.9	-5.1
100	89.9	-10.1
110	93.8	-16.2
120	97.4	-22.6
130	100.5	-29.5
140	103.2	-36.8
150	105.8	-44.2
160	107.9	-52.1
170	109.3	-60.7
177.7	110.3	-67.4

Table 2. Simulated slacked off weight at the surface vs. at the liner's packer depth

Fig. 3. Representing the flowing effect on the drillpipe wiper.

were deformed against the inside diameter (ID) of the drillpipe in a flowering effect, Fig. 3.

CURRENT IMPROVED PRACTICES

Manganese Trioxide (Mn_3O_4) Mud System

The introduction of a new manganese trioxide *(Mn_3O_4)* mud system had resolved several limitations with the barite-only system, thereby reducing the complexity of the deployment of the liner hanger system. For example, the Mn_3O_4 system has a lower solid percentage compared with the barite-only system[3]. Additionally, because of the spherical and consistent shape of the particle sizes, the Mn_3O_4 exhibits lower and more consistent rheological values. Having a lower rheological value, e.g., plastic viscosity and yield point, helped reduce the ECD during running and cementing of the liner, which decreased the chance of having losses. Table 3 shows that within the same MW, the Mn_3O_4 mud shows a 2.5 pcf reduction in ECD, and 3% less of solid content in the mud. Additionally, the sagging effect occurrence with this mud was negligible if compared with the barite-only system[4].

In addition, this mud assisted in deploying the liner hanger as follows:

- The lower the solid content in mud, the less likely is the chance of forming a film across the casing. This in return makes it easier to set the liner hanger slips.
- Reduced the chances of having settlement in the liner hanger hydraulic ports, which increases the chances of being able to set the liner without issues.
- Reduced the chances of having a malfunction within the float equipment due to a barite settlement. This is especially important in case of using MPC where having floats is necessary to be able to apply annular back pressure on the formation.

Furthermore, to ensure the rheology of the mud was kept in control at all times during the drilling, running, and cementing

MW (pcf)	MW (ppg)	Mud Type	Solid Content (%)	PV	YP	ECD
145	19.38	Mn_3O_4	42	30	20	150
		Barite	45	53	24	152.5

Table 3. Mud properties with different mud type[4]

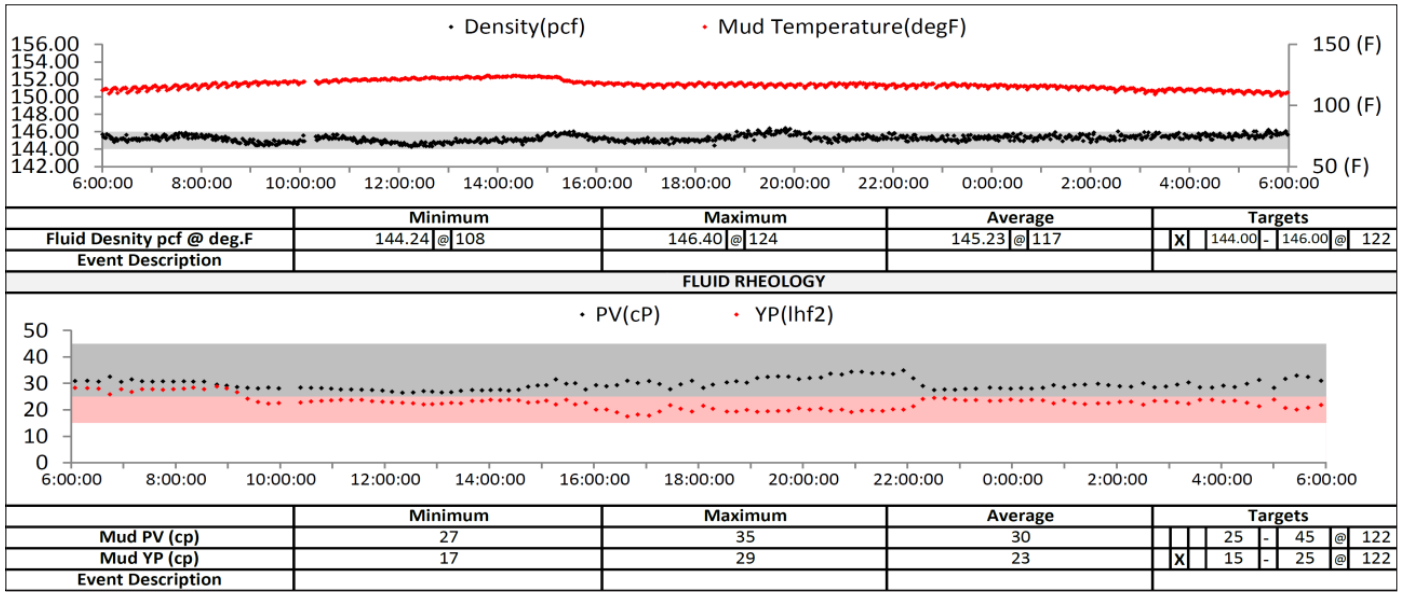

Fig. 4. An example of the automated daily mud monitoring system readings.

of the liner, an automated mud monitoring system was used. This system is meant to monitor the rheology of the mud every 15 minutes and the MW every 1 minute. Figure 4 is an example of the automated mud daily report where it shows the rheology and MW continuously.

MPC

As mentioned earlier, the tight MW window in this field is a challenge not only during drilling, but also during cementing as well. For that reason, several methods were used to reduce the bottom-hole pressure, and notably MPC was one of them. During MPC, the cement job is typically performed by using underbalance (or near balance) MW to avoid losses during the cement job. The typical pieces of equipment that are used for the MPC includes a rotating circulating device (RCD), hydraulic chokes, float equipment in the liner, and flow out meters.

In addition to MPC, controlling the ECD while tripping is important. This is done by controlling the tripping speed to minimize the surge pressure on the formation, and also by displacing the string to lower MW while running in hole in stages to minimize the ECD[1].

Liner Hanger System Improvements

Lessons learned from previous experiences from extreme downhole conditions were applied during the preparation of the liner equipment. A combination of multiple practices improved significantly the liner hanger setting success. One of them was the utilization of a high temperature grease to reduce the chances of solids settlement on the slips. More importantly, the type of liner hanger deployed in the field utilized the most recent design improvements for the hanger system, which included an optimized slip seat wedge profile and slip rail design for increased resilience to solids packing off while at the same time providing a stronger hanging lip/slip seat interface.

At the running tool, a unique arrangement of sealing cups was used to protect the setting port of the hanger from being clogged by the high solids content mud. In addition, proper BHA selection during running the liner, or the tie back packer, is critical to provide sufficient weight transmission to the liner. The running tool was rotated during the setting of the packer to provide a more efficient weight transmission to the packer at the setting depth. In most of the cases, the hanger was set in the first attempt with no difficulties.

With respect to the "flowering effect" of the drillpipe dart and the incident related with the cement displacement, it was noticed that the plug used for the job covered a wide range of drillpipe ID, allowing fluid to be bypassed through the wiper fins in a heavier weight drillpipe, due to flowering. For this reason, a dart with rubber fins with an optimum OD more compatible to the drillpipe used in the field — 5½" 24.7 lb/ft XT-54 — was introduced. The fins of this drillpipe wiper provide a better contact to the drillpipe ID without excessive

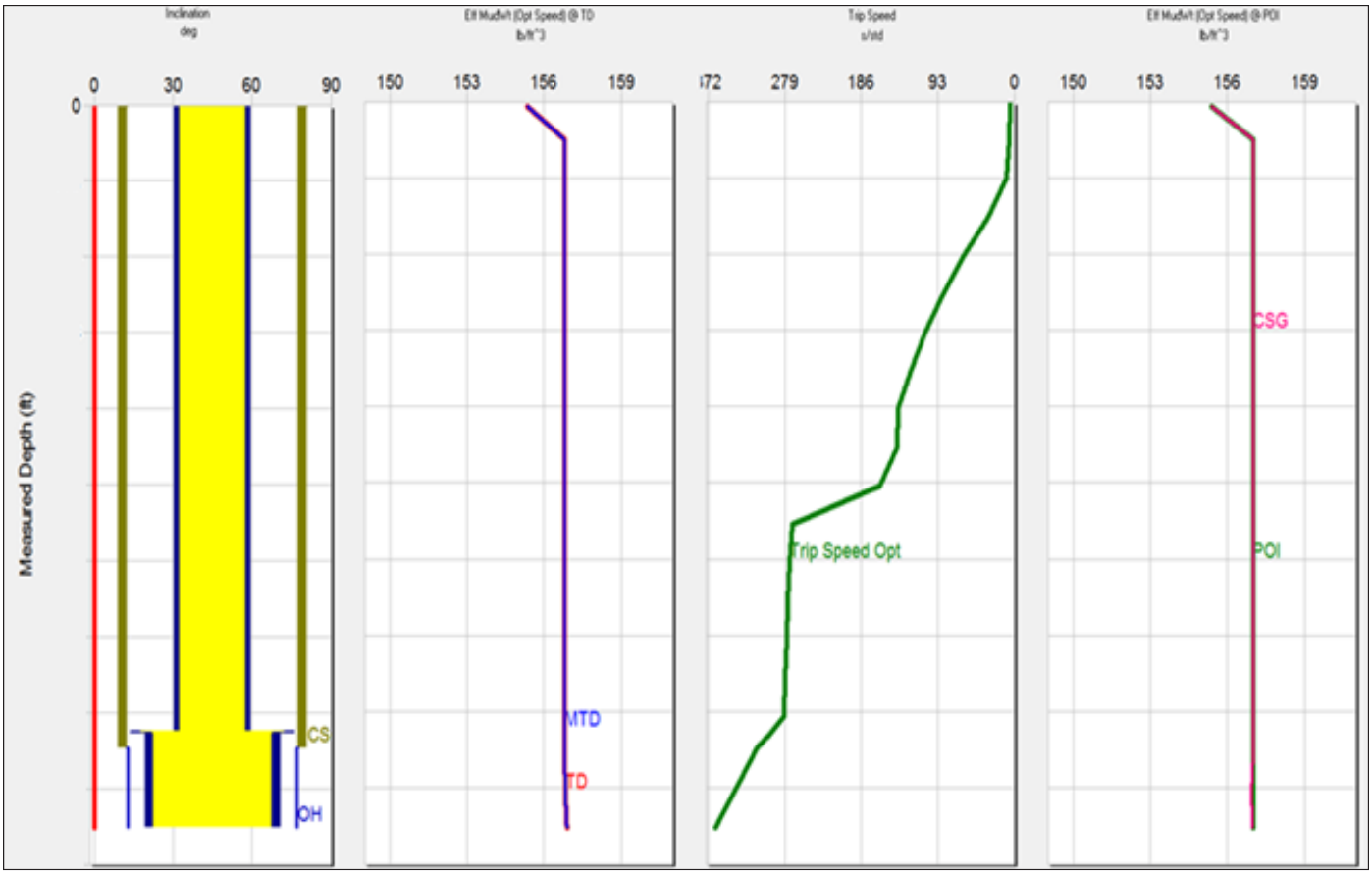

Fig. 5. An example of the running speed simulation that goes into the preplanning phase prior to running the liner.

compression of the rubber, thereby reducing the chances of the flowering effect mentioned earlier.

Controlling the ECD to Minimize Fluid Losses

Detailed pre-job planning and simulations were prepared to reduce frictional pressures to a minimum, and to prevent drilling fluid losses while running the liner in the hole and while pumping and displacing cement. The liner running speed strictly followed the results of the pressure surge simulations, Fig. 5.

In addition, keeping the fluid in continuous motion by frequently breaking the mud gels also assisted in maintaining the ECD within the calculated limits, and at the same time reduced the chances of solids settling in the float equipment that could lock open the float valves. The continuous monitoring of the pressure while circulating helped in identifying trends of high pressure that required longer circulating times until the pressure stabilized.

The actions described here assisted significantly in reducing the occurrence of fluid loss while the liner was being deployed, and thereby improving the chances of a better cementing job.

Planning for the Worst Case in Cases of Fluid Losses

Experiencing severe or total fluid losses during the cement job resulted in not only having a poor cement isolation in the annulus, but it also had the direct effect of exerting the considerable forces of ballooning and piston effect against the hold down slips of the liner's top packer. With this knowledge that the current liner top packer had a limitation when subjected to a negative test as part of an uncemented liner, it was decided that in case the cement job was performed with severe and/or total fluid losses occurring, then a liner top packer would be set for the purpose of providing a temporary well control barrier only. A tie back packer, with a greater hold down capability that covered the possible force during a negative test on an uncemented liner system, would be set on top of the liner in a separate trip. Following the installation of the tie back packer, the negative test was performed using the second tie back packer as a barrier, and the main isolation system at the liner top.

Transferring set down weight on the S-shape of the well profile was a continuous challenge. Despite having a setting string that was heavy enough at the surface to be able to slack off a minimum 70 Klb of weight, to set the hold down slips, the results showed that on some occasions it was insufficient to set the packer. An optimized BHA, which included drill collars and heavy weight drillpipe, was planned with the purpose of reducing the buckling and increasing the stiffness and to enable the packer slips to be set. As a standard procedure, it required a slack off weight of up to 120 Klb at the surface. Rotation of the string was mandatory as this also decreases buckling of the string. Packers deployed using these measures were flawlessly installed and later tested with no further failures.

DEPLOYMENT OF A LINER SYSTEM WELL-A

In Well-A, the 9⅝" casing was set 1,000 ft above the high-pressure zone. The well was drilled with MPD with 145 pcf MW and 152 pcf ECD. The well was displaced into two stages to 152 pcf; first stage at the bottom, and second stage at the casing shoe. The BHA was pulled out of hole and the 7" liner was run as follows:

1. The 7" hydraulic liner hanger was deployed with the latest engineered modifications on this well, such as use of the optimized design of the liner hanger slips to tolerate excessive high solids content, high temperature grease on the running tool and liner hanger system, special running tool arrangement for handling fluids with high solids content, and drillpipe wiper fins adjustment, etc.
2. After picking up the liner hanger, the well was displaced with a fresh Mn_3O_4 mud, without loss circulation materials, to avoid mud settlement inside the liner hanger ports — required for activating the slips.
3. The tripping speed was planned as 8 minutes per stand in the cased hole and 10 minutes per stand in the open hole to avoid exceeding an ECD of 153 pcf.
4. At the casing shoe, the RCD was installed, and the well was displaced to 150 pcf.
5. The ECD was closely monitored and the liner was washed down to the bottom in the open hole. The liner reached the bottom, neither encountering hole problems nor fluid losses. The well was circulated clean in preparation for setting the liner hanger.
6. The liner hanger was set hydraulically from the first attempt by dropping a brass ball and pressuring the system to ±1,800 psi and slacking off the weight on the liner slips. Also, the running tool was released hydraulically by dropping a larger ball and pressuring the system to ± 2,200 psi and blowing the ball seat. There was no restriction of flow or loss circulation after blowing the ball seats of the liner hanger system.
7. With MPC equipment rigged up, the well was cemented with 160 pcf of Micromax cement and 155 pcf spacer. The drillpipe wiper plug was pumped as per the displacement calculation and the liner floats were holding — no flow back was observed. No fluid losses were experienced.
8. Upon finishing the cementing job, the liner packer was set while rotating the drillpipe, to provide sufficient weight to the liner. A good indication was observed at the surface that the liner's top packer was set.
9. After pulling out of hole with the running tool, and as a precautionary measure to avoid a leak through the liner's top packer, a second tie back packer was deployed. Before running the tie on packer, the proper BHA with enough drill

collar and heavy weight drillpipe was selected, to be able to transfer sufficient weight to the slips.

10. A negative test was done by setting a testing packer on top of the liner, and displacing the well from 150 pcf to 64 pcf (water weight) in stages. Both the tie on packer and the liner packer passed the negative test.
11. The next hole section was drilled to section total depth. Subsequently, the well was completed and then displaced to completion fluid without having any issue with the 7" packer leaking.

CONCLUSIONS

1. Implementing the liner modification and practices reduced the NPT on those high-pressure, high temperature wells. An estimation savings of ±30 days was made by avoiding the wet shoe failures and liner top repairs.
2. The Mn_3O_4 mud reduced the solid content in the mud system, and therefore reduced the problems seen with the barite system, e.g., barite settlement, high gel values, mud losses, etc.
3. ECD control practices, e.g., MPC, controlling tripping speed, and multistage displacement, significantly helped in avoiding the losses during running and cementing of the liner, which in return, increased the support to the liner packer.
4. The pressure balanced liner hanger system allowed for circulation without pressure limitations with these drilling fluids that contain high concentrations of solids.
5. Proper BHA selection was critical for weight transferring downhole to the packer depth, to have proper setting for the packer for this S-shape casing design. Additionally, rotating the pipe — if possible — helped effectively transmit the weight.

ACKNOWLEDGMENTS

The authors would like to thank the management of Saudi Aramco and Baker Hughes, a GE company, for their support and permission to publish this article.

This article was presented at the SPE Annual Technical Conference and Exhibition, Dallas, Texas, September 24-26, 2018.

REFERENCES

1. Aljubran, M.J., Oqaili, A.H., Ezi, P.C. and Iturrios, C.O.: "Utilizing a Fully Automated MPD System to Run and Cement 9⅝" Liner String in HPHT Gas Wells," SPE paper 190006, presented at the SPE/IADC Managed Pressure Drilling and Underbalanced Operations Conference and Exhibition, New Orleans, Louisiana, April 17-18, 2018.
2. Ezzat, A.M., Jennings, S.S., Al-Abdulgader, K.A. and Al-Hammad, M.A.: "Application of Very Heavy Mud and Cement in a Wildcat," SPE paper 62802, presented at the IADC/SPE Asia Pacific Drilling Technology, Kuala Lumpur, Malaysia, September 11-13, 2000.
3. Gadalla, A., Pino, R., Ezi, P.C., Zayer, N., et al.: "High Density Fluids Customization and Field Application in Khursaniyah Challenging Wells," SPE paper 183997, presented at the SPE Middle East Oil and Gas Show and Conference, Manama, Kingdom of Bahrain, March 6-9, 2017.
4. Alrasheed, A., Oqaili, A.H., Aljubran, M.J. and Ezi, P.C.: "Deployment of Fully Automated MPD and Manganese Tetroxide Mud System to Drill Ultra-Narrow Mud Window in HPHT Gas Wells," SPE paper 190000, presented at the SPE/IADC Managed Pressure Drilling and Underbalanced Operations Conference and Exhibition, New Orleans, Louisiana, April 17-18, 2018.

BIOGRAPHIES

Abdullah H. Oqaili is currently working as a Drilling Engineer in Saudi Aramco's Gas Drilling Engineering Department. He has more than 6 years of experience and has worked in several onshore and offshore oil and gas fields throughout Saudi Arabia.

Abdullah received his B.S. degree in Petroleum Engineering from Missouri University of Science and Technology, Rolla, MO.

He is an active member of the Saudi Council of Engineers (SCE), and the Society of Petroleum Engineers (SPE).

Abdulaziz S. Alluhaydan is currently working as a Drilling Engineer in Saudi Aramco's Gas Drilling Engineering Department. He has more than 8 years of experience and has worked in several onshore gas fields throughout Saudi Arabia. Abdulaziz worked with Schlumberger as a Logging While Drilling (LWD)/Measurement While Drilling (MWD) Field Engineer in Oman for 15 months as a part of a co-op training program with Saudi Aramco.

He received his B.S. degree in Petroleum Engineering from Texas Tech University, Lubbock, TX.

Abdulaziz is an active member of the Saudi Council of Engineers (SCE), and the Society of Petroleum Engineers (SPE).

Peter C. Ezi is an Acting General Supervisor with Saudi Aramco's Northern Area Onshore Gas Drilling Engineering Division of the Gas Drilling Engineering Department. Peter has 26 years of oil and gas industry experience. Before joining Saudi Aramco in 2008, he worked for the Shell Petroleum Development Company (SPDC) of Nigeria.

While working at SPDC, Peter gained experience in drilling operations, which includes complex well planning, design and construction, drilling contracting services, business planning and budgeting, and well performance management. He was also involved in the planning phase of the EA shallow offshore field development drilling project, slim well drilling operation, land rig and coiled tube drilling combination in marginal reservoirs, field testing of high rate gravel pack and the onshore TUNU/Kanbo drilling and completion campaign for the early production facility in SPDC.

In addition to his responsibilities in Saudi Aramco, Peter championed the innovative drilling strategy for the Jauf wells in the Shedgum field using 5½" polished bore receptacle monobores, the first deployment of a flute hanger wellhead in Saudi Arabia, and the first implementation of an incentive program in the Gas Development Drilling Department. He has been instrumental in the development of young engineers in the Professional Development Program through mentoring and coaching.

Peter received his B.S. degree in Chemical Engineering from Anambra State University of Technology, Enugu, Nigeria.

Alvaro Tirado joined Baker Hughes, a GE company, in 2000. Currently, he is working as the Regional Technical Manager for Wellbore Construction, covering the Middle East, North Africa, Turkey, and India (MENATI) areas. Alvaro has over 21 years of experience in the oil industry and he has served in various positions in Latino America and the Middle East.

Alvaro's area of expertise is on technical support, implementation of processes and managing projects for completions. Working with major operators in five different countries, he has executed critical developments in areas with high liner hangers' activities like deepwater wells, extended reach drilling, and high-pressure, high temperature environments. In Alvaro's previous role, he served as the Operations Manager for Wellbore Construction for Gas Land operations in Saudi Arabia.

Alvaro received his B.S. degree in Petroleum Engineering from the Universidad Industrial de Santander, Bucaramanga, Santander, Colombia.

Further Insight into Calcium Carbonate Scale Inhibition at High Temperature

Dr. Qiwei Wang and Dr. Tao Chen

ABSTRACT

Threshold inhibitors are commonly used to prevent scale formation in oil field production systems. Effective scale control still remains a significant challenge under harsh environmental conditions such as high temperatures. The risk of calcium carbonate ($CaCO_3$) scale deposition is increased with higher temperatures by the inverse solubility behavior, which will accelerate the precipitation kinetics; while the inhibitor performance deteriorates with thermal degradation, incompatibility with produced water, and decreased inhibition efficiency. Although extensive works have been devoted to study the $CaCO_3$ inhibition behavior, the performance of inhibitors under harsh conditions is still not fully understood.

This article presents a study of different types of inhibitors at high temperature. Evaluation tests are conducted using a dynamic tube blocking method. High calcium tolerance generic inhibitors with various molecular structures are studied at 150 °C. The inhibitors include organic phosphate, co-polymers with various function groups, and environmental friendly chemicals. The brine composition is varied by changing the scaling ion ratio over a wide range. Test results indicate that the effectiveness of inhibitors can be significantly affected by the brine composition, even at the same $CaCO_3$ saturation state. In general, the inhibitor performance increases with calcium concentration in the test brine, and the performance ranking of different inhibitor chemistry also changes with brine composition. The results indicate that the effect of the scaling ion ratio must be considered in scale risk assessments and for the optimization of a treatment program.

INTRODUCTION

Calcium carbonates ($CaCO_3$) are the predominant scale type formed during oil and gas production[1, 2]. Its formation is largely caused by pressure reduction. A decrease in pressure causes the shift in chemical equilibrium among produced fluids (oil, water, and gas). As the pressure drops, dissolved carbon dioxide (CO_2) gas in produced water evolves into a gas phase, leading to a higher pH value, which shifts the water to supersaturated in regard to $CaCO_3$, and consequently, the precipitation of $CaCO_3$ scale[3]. The $CaCO_3$ scaling risk increases with temperature, due to its reverse solubility behavior. Figure 1 shows the solubility behaviors of three $CaCO_3$ polymorphs — calcite, aragonite, and vaterite.

$CaCO_3$ scale can restrict fluid flow, cause formation damage, and damage equipment. Figure 2 shows $CaCO_3$ scale deposited on electric submersible pump (ESP) parts in an offshore oil field, which leads to the premature failure of ESP systems[5]. Figure 3 illustrates the production rate decline due to $CaCO_3$ accumulation in sand screen and near wellbore areas in one high temperature gas well.

The use of threshold inhibitors is widely practiced to prevent scale formation. Such inhibitors in trace amounts can disrupt nucleation, retard growth or alter morphology of scale crystals, which could otherwise agglomerate and form hard deposits. Many studies have been performed to evaluate the performance of $CaCO_3$ scale inhibitors under varying conditions. The impacts of various parameters, including supersaturation state,

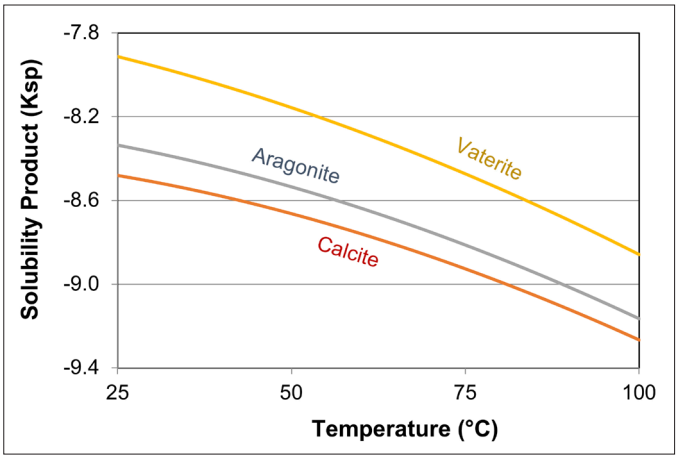

Fig. 1. Changes of $CaCO_3$ solubility with temperature[4].

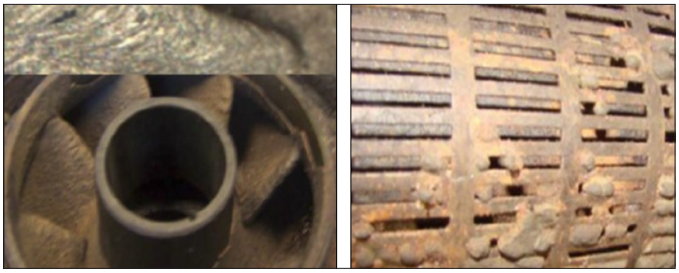

Fig. 2. $CaCO_3$ scale on an ESP pump stage (left) and intake (right).

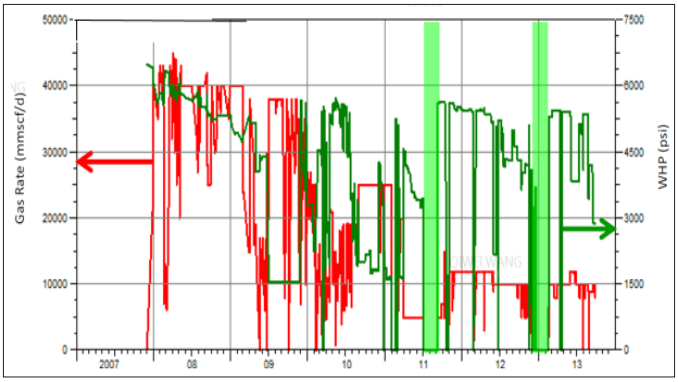

Fig. 3. Changes of gas production rate and wellhead pressure due to $CaCO_3$ scale accumulation.

temperature, flow rate, impurities, chemical additives, and surface properties, have been investigated[6-13]. In the present work, the performance of some commonly used inhibitors are investigated at high temperature — 150 °C — with different brine compositions.

EXPERIMENTAL

Synthetic brines were used throughout this study. The chemical compositions of test brines are listed in Table 1. These brines were selected because they had very different calcium to bicarbonate ratios. The calcium concentration was changed from 8,200 mg/L in Brine #1 to 700 mg/L in Brine #2, and 110 mg/L in Brine #3, while the bicarbonate content was increased from 150 mg/L in Brine #1 to 700 mg/L in Brine #2, and 3,000 mg/L in Brine #3, which represented the scaling ion ratio of calcium to bicarbonate (in ppm) from > 50 in Brine #1 to 1.0 in Brine #2, and < 0.05 in Brine #3. All of these brines have the same supersaturation stage with respect to calcite, with a saturation index (SI) of 2.57 under test conditions (150 °C and 300 psi), based on the calculation using a JIP sponsored prediction model[14].

Reagent grade chemicals were used to prepare the synthetic brines. Cation brine, which contained calcium and magnesium chloride salts, and anion brine, which had sodium chloride, were prepared separately. A mixture of equal volumes of cation and anion brines resulted in the desired test brine composition. The prepared brines were then filtered through 0.45 µm filter paper and degassed under a vacuum for at least two hours before use. Bicarbonate salt ($NaHCO_3$) was added into the

Parameter	Brine #1	Brine #2	Brine #3
Ca^{2+} (mg/L)	8,200	700	110
Mg^{2+} (mg/L)	50	50	50
Na^{+} (mg/L)	2,000	10,600	12,257
HCO_3- (mg/L)	150	700	3,000
Cl- (mg/L)	17,630	17,330	14,076
pH	7.2	7.7	7.9

Table 1. Test brine compositions used in the study

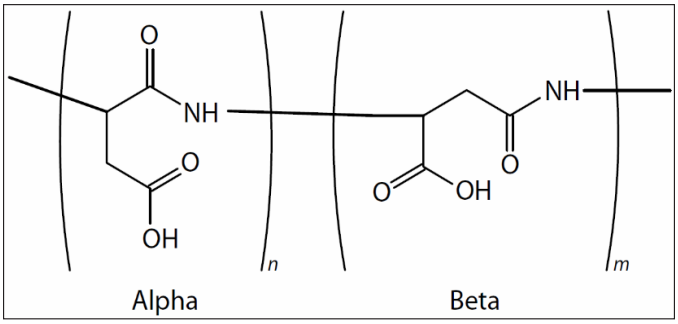

Fig. 4. Molecular structure of the SI-B inhibitor.

anion brine after the degassing treatment to minimize the pH change, due to the loss of dissolved CO_2 gas.

The scale inhibitors tested include phosphonate (SI-A), polyaspartate (SI-B), a polymaleic-based co-polymer (SI-C), and a sulfonated polyacrylate co-polymer (SI-D). All inhibitors were commercial products and used without further purification. SI-B is an environmental friendly inhibitor and its molecular structure is shown in Fig. 4.

Evaluation tests were carried out using the dynamic tube blocking designed to provide a dynamic condition for scale formation and inhibition with the temperature at 150 °C and a back pressure of 300 psi. The method operated under the principle that scale buildup on the interior surface of a small capillary increases the pressure drop across the capillary. Figure 5 is a schematic drawing of the scale inhibitor test rig. The system consisted of three high performance liquid chromatography pumps, A, B, and C. They were used for cation brine (pump A), anion brine (pump B), and inhibited anion brine (pump C).

A change in inhibitor concentration during test runs was achieved by adjusting the flow rates of pumps B and C. The combined flow rates of these two pumps were kept at 5 ml/min — the same as pump A. Brines from pumps B and C were mixed prior to a preheating coil. Then preheated cation and anion brines were comingled in a mixing chamber in front of the scaling coil (Monel alloy, 1 mm internal diameter, 1 m in length). Differential pressure (ΔP) across the scaling coil was continuously monitored and recorded, along with the mixing chamber temperature and back pressure. The formation of a $CaCO_3$ deposit was indicated by an increase in ΔP, due to a

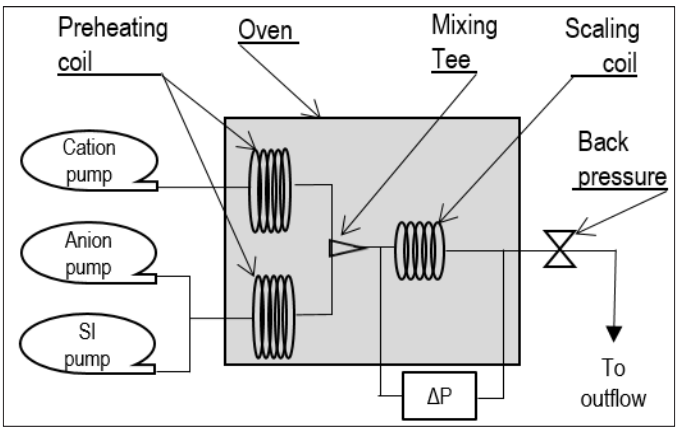

Fig. 5. Schematic drawing of scale inhibitor test rig.

reduced cross-section area. The deposition induction period was defined as the amount of time elapsed between the beginning of the test run to the onset of ΔP showing a speed increase, and scaling time was determined as the time elapsed to a ΔP increase, reaching 1 psi.

The blank scaling time was established first for each test brine, and the scaling time was defined as the elapsed time for the ΔP increase to reach 1.0 psi. Then the minimum effective dose (MED) was determined for each inhibitor product. In each test, the inhibitor concentration was reduced stepwise after ~2.5 times of blank scaling time. The MED was the lowest inhibitor concentration at which the ΔP showed less than 1.0 psi increase over the test period. At the end of each run, the scaling coil was cleaned with 10% acetic acid for 30 minutes, followed with deionized water for at least 2 hours to remove $CaCO_3$ blockage and any residual inhibitor.

RESULTS AND DISCUSSION

Highly repeatable blank scaling times were achieved for all three test brines, with a variation within 0.5 minutes in the duplicate tests. Selected results are presented in Fig. 6. With high test temperature and high supersaturation, $CaCO_3$ scale formed quickly in the capillary coil. The medium calcium and bicarbonate Brine #2, and low calcium/high bicarbonate Brine #3, had similar scaling times of around 6 minutes, which was much faster than the high calcium/low bicarbonate Brine #1, which scaled after about 12 minutes. These results indicate that although with same thermodynamic driving force for $CaCO_3$ precipitation, the scaling rate could vary significantly with changes in the scaling ion ratio.

The scaling ion ratio had a more pronounced influence on the scale inhibition. For Brine #1, all tested inhibitor products were effective at 10 ppm and no ΔP changes were recorded over the 30 minute test duration, Fig. 7. Inhibitors based on SI-B and SI-D failed when their concentration was reduced to 7.5 ppm, although, phosphonate (SI-A) and polymaleic co-polymer (SI-C) inhibitors were more effective. $CaCO_3$ scale deposition was completely prevented with 5 ppm of inhibitor SI-A or

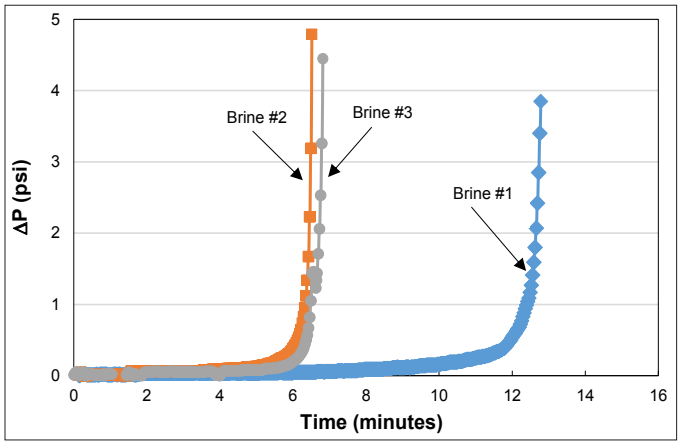

Fig. 6. Test results for the blank brines.

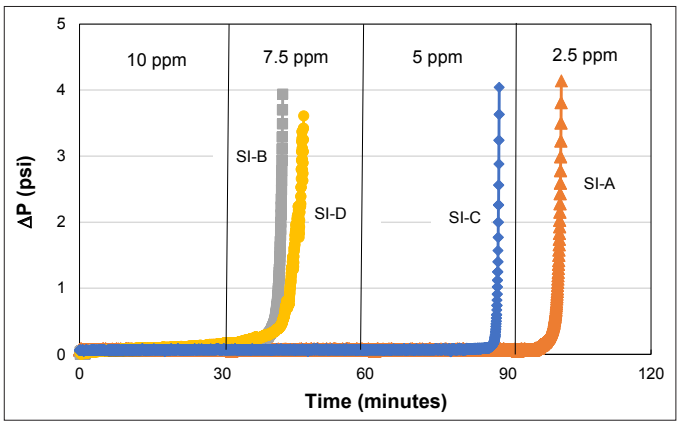

Fig. 7. Scale inhibitor performance in the high calcium/low bicarbonate brine, Brine #1.

7.5 ppm of inhibitor SI-C. The performance ranking was: SI-A > SI-C > SI-D ≥ SI-B.

Much higher inhibitor concentrations were required to prevent $CaCO_3$ scale in Brine #2, despite the test duration being reduced to 15 minutes, Fig. 8. The ΔP started to increase when the inhibitor concentration was decreased from 90 ppm to 75 ppm for SI-B and SI-D, and to 60 ppm for SI-A and SI-C, suggesting the onset of $CaCO_3$ deposition. The ΔP increase surpassed 1 psi at 60 ppm for SI-B and SI-D, 45 ppm for SI-C, and 15 ppm for SI-A. The MED values were more than five times higher than that determined in the high calcium/low bicarbonate brine, Brine #1. The performance ranking was similar to Brine #2: SI-A > SI-C > SI-B ≥ SI-D.

Furthermore, scale inhibitors became less effective in brine with much higher bicarbonate than calcium such as Brine #3, particularly for inhibitors SI-A and SI-C. Both SI-A and SI-C showed lower inhibition efficacies than inhibitors SI-B and SI-D, in contrast in Brine #1 and Brine #2. Inhibitor SI-A failed at 120 ppm and inhibitor SI-C failed at 100 ppm, while the MED values for inhibitors SI-B and SI-D showed slight increases over Brine #3, Fig. 9. The relative performance was: SI-D > SI-B > SI-C > SI-A.

The determined MED results are summarized in Fig. 10, which clearly shows the impact of the calcium to bicarbonate

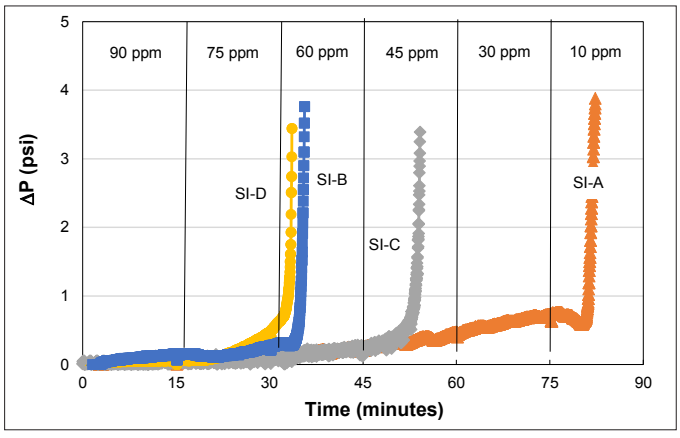

Fig. 8. Scale inhibitor performance in the medium calcium/medium bicarbonate brine, Brine #2.

ratio on scale inhibitor effectiveness. These results suggest that the scaling ion ratio must be considered in the selection of the inhibitor product and development of a treatment program. Figure 11 summarizes the measured calcium and bicarbonate concentrations of produced waters in a gas field. Wide ranges of water chemistry variations were observed, with the calcium concentration changed from < 500 mg/L to > 25,000 mg/L, and the bicarbonate content varied from < 100 mg/L to ~750 mg/L. These lead to a change of the calcium to bicarbonate ratio from < 0.1 to 80. Based on this study, the inhibitor treatment dosage must be increased for these wells, which produced water with a low calcium to bicarbonate ratio.

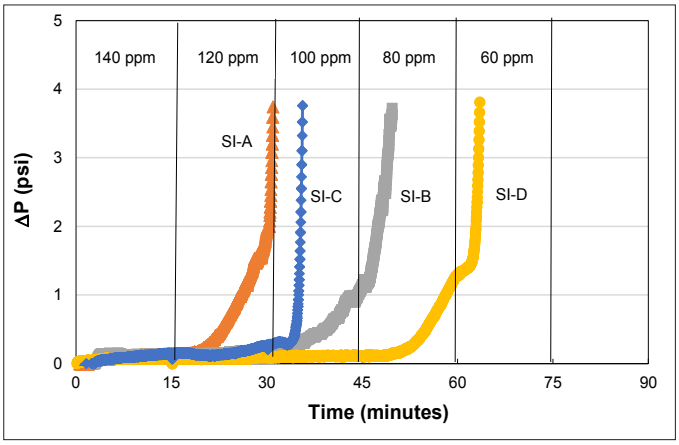

Fig. 9. Scale inhibitor performance in the low calcium/high bicarbonate brine, Brine #3.

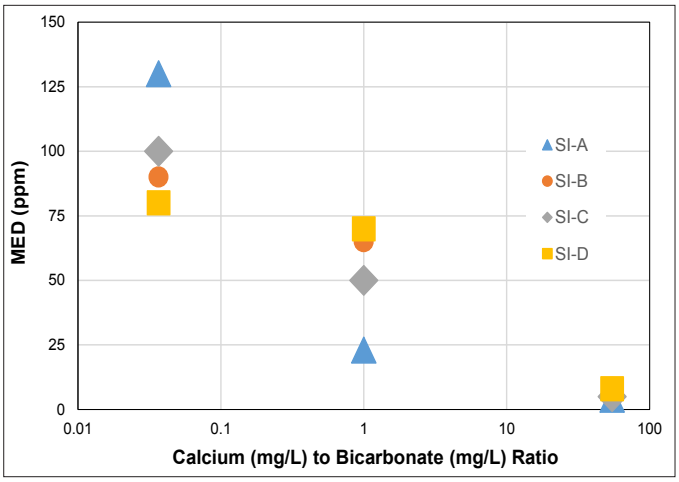

Fig. 10. Summary of test results that illustrate the impact of brine composition on scale inhibitor performance.

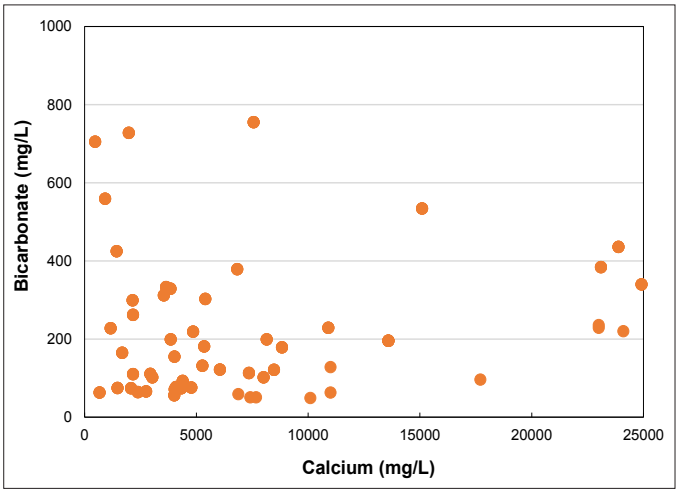

Fig. 11. Calcium and bicarbonate concentrations of produced waters in a gas field.

CONCLUSIONS

Results from this study show that the effectiveness of a scale inhibitor at high temperature is very sensitive to brine composition. All scale inhibitors studied are much more effective in a high calcium brine. Brines with low calcium, but elevated bicarbonate ions, are more difficult to inhibit than the brines rich in calcium. The relative performance ranking of different types of inhibitors is also affected by the scaling ion ratio, e.g., SI-A and SI-C, which becomes much less effective in bicarbonate-rich brines than in calcium-rich brines. For a given oil well, the scaling ion ratio in produced water can vary substantially if the calcium concentrations in connate water and injection water are very different. Therefore, the impact of the scaling ion ratio should be considered in a scale risk assessment, and for the optimization of the treatment program.

It is interesting to note that the inhibitor chemical based on polyaspartate, an environmental friendly compound, is more effective than the commonly used phosphonate and polymer products in a low calcium brine.

ACKNOWLEDGMENTS

The authors would like to thank the management of Saudi Aramco for their support and permission to publish this article.

REFERENCES

1. Hinrichsen, C.J.: "Preventing Scale Deposition in Oil Production Facilities: An Industry Review," paper 98061, presented at the NACE International/CORROSION 1998 Conference and Exposition, San Diego, California, March 22-27, 1998.
2. Cowan, J.C. and Weintritt, D.J.: *Water-Formed Scale Deposits*, Gulf Publishing Co., Houston, Texas, 1976, 606 p.
3. Raju, K.U.: "Successful Scale Mitigation Strategies in Saudi Arabian Oil Fields," SPE paper 121679, presented at the SPE International Symposium on Oil Field Chemistry, The Woodlands, Texas, April 20-22, 2009.
4. Plummer, L.N. and Busenberg, E.: "The Solubilities of Calcite, Aragonite and Vaterite in CO_2-H_2O Solutions between 0 and 90 °C, and an Evaluation of the Aqueous Model for the System $CaCO_3$-CO_2-H_2O," *Geochimica et Cosmochimica Acta*, Vol. 46, Issue 6, June 1982, pp. 1011-1040.
5. Wang, Q., Zaidi, S., Al-Nasser, W., Shepler, R., et al.:

"Solids Deposition in Electric Submersible Pumps and Treatment Strategies," paper MECC FEB16-8171, presented at the 16th Middle East Corrosion Conference and Exhibition, Manama, Kingdom of Bahrain, February 8-11, 2016.

6. He, S., Kan, A.T. and Tomson, M.B.: "Inhibition of Calcium Carbonate Precipitation in NaCl Brines from 25 to 90 °C," *Applied Geochemistry*, Vol. 14, Issue 1, January 1999, pp. 17-25.
7. Chen, T., Neville, A., Sorbie, K. and Zhong, Z.: "In-Situ Monitoring the Inhibiting Effect of DETPMP on $CaCO_3$ Scale Formation by Synchrotronx-Ray Diffraction," paper 07053, presented at the NACE International/CORROSION 2007 Conference and Exposition, Nashville, Tennessee, March 11-15, 2007.
8. Fielder, G.D.: "Scale Inhibitor Selection for a High Suspended Solids Produced Water System," paper 00105, presented at the NACE International/CORROSION 2000 Conference and Exposition, Orlando, Florida, March 26-31, 2000.
9. Wang, Q., Al-Dawood, F. and AlSaiari, H.: "Carbonate Scale Formation and Inhibition in the Presence of Zinc Ions," *Materials Performance*, Vol. 51, Issue 11, November 2012, pp. 60-64.
10. Wang, Q., Al-Badairy, H., Shen, S. and Al-Nasser, W.: "Calcium Carbonate Scale Formation and Inhibition during Enhanced Oil Recovery," *Materials Performance*, Vol. 56, Issue 3, March 2017, pp. 48-51.
11. Lu, H., Alattal, F., Ruggeri, J., Brooks, J., et al.: "Iron Effects on Scale Inhibitor Performances for Laboratory and Field Operations," paper 7771, presented at the NACE International/CORROSION 2016 Conference and Exposition, Vancouver, British Columbia, Canada, March 6-10, 2016.
12. Alwi, N.B., Salleh, I.K., Ibrahim, J.M., Carpenter, I., et al.: "Development of Improved Chemical Formulations for Scale Control for Alkaline Surfactant Polymer Flood in a Seawater Flooded Reservoir," SPE paper 179883, presented at the SPE International Oil Field Scale Conference and Exhibition, Aberdeen, Scotland, U.K., May 11-12, 2016.
13. Vazirian, M.M., Charpentier, T.T.J., Neville, A., Alvim, F.B., et al.: "Assessing Surface Engineering Solutions for Oil Field Scale; Correlating Laboratory Tests to Field Trial," SPE paper 179862, presented at the SPE International Oil Field Scale Conference and Exhibition, Aberdeen, Scotland, U.K., May 11-12, 2016.
14. Kan, A.T. and Tomson, M.B.: "Scale Prediction for Oil and Gas Production," SPE paper 132237, presented at the International Oil and Gas Conference and Exhibition in China, Beijing, China, June 8-10, 2010.

BIOGRAPHIES

Dr. Qiwei Wang works in Saudi Aramco's Research & Development Center as a Science Specialist in oil field scale mitigation. Since joining Saudi Aramco in 2011, he has played a key role in all major scale mitigation activities and led the completion of over 40 projects. Before joining Saudi Aramco, Qiwei worked for Nalco Champion as a R&D Coordinator on flow management and as a Senior Specialist on scale management. He has over 25 years of R&D and technical support experience in oil field production chemistry, scale management, and water treatment.

Qiwei is an active member of the Society of Petroleum Engineers (SPE) and National Association of Corrosion Engineers (NACE). He has organized workshops, served on technical committees and chaired several conferences for both organizations.

He has authored and coauthored over 130 publications and 12 U.S. patent applications.

Qiwei received his B.Eng. degree in Chemical Engineering from Taiyuan University of Science and Technology, Taiyuan, China; an M.Eng. degree in Material Sciences from Harbin Institute of Technology, Harbin, China; an M.S. degree in Chemistry from the University of Ryukyus, Okinawa, Japan; and a Ph.D. degree in Oceanography from Texas A&M University, College Station, TX.

Dr. Tao Chen is a Petroleum Engineering Specialist working with the Production Technology Team of Saudi Aramco's Exploration and Petroleum Engineering Center – Advanced Research Center (EXPEC ARC). His interests are production chemistry and flow assurance in the oil and gas industry, specializing in oil field scale management.

Prior to joining Saudi Aramco in 2014, Tao spent more than 15 years on oil field scale management and worked at Clariant, Champion Technologies, Nalco Champion, and LR Senergy in Aberdeen, U.K.

He has published nearly 70 technical publications about scale management in oil fields.

Tao received both his B.S. and M.S. degrees in Chemical Engineering from Dalian University of Technology, China, and his Ph.D. degree in Chemical Engineering from Heriot-Watt University, Edinburgh, U.K. Tao also received an MBA from Warwick University, Coventry, U.K.

Integrated 3D Geomechanics Model to Characterize the in Situ Stress Rotations and their Implications on the Mechanical Behavior of the Natural Fractures and Drilling Operations: A Case Study for a Carbonate Reservoir, Saudi Arabia

Dr. Tariq Mahmood, Otto E. Meza Carmargo, Ali H. Al-Gawas, Khalid A. Al-Hawas, Abdulrazaq Reda Nashar, Dr. Ivan Deshenenkov, and Carlos A. Planchart

ABSTRACT

This work presents the determination of the in situ stress field of a carbonate reservoir in a complex tectonic area within the Arabian Plate. The detailed determination of the stress field is important to field characterization as it controls the fundamental mechanical behavior of open and closed fractures. The presence of open natural fractures can have an adverse effect on drilling operations, e.g., "total loss circulation," etc. An integrated 3D geomechanical model was built to characterize the rock mechanical properties and the stress orientations to analyze the behavior of natural fractures and micro-faults under the current state of stress.

The workflow used in this study combines the analysis from multidisciplinary sources, including wireline logs, drilling data, borehole images, dipole sonic, borehole seismic, core triaxial tests, 1D mechanical earth models (MEM), critical stressed fractures and 3D seismic attribute analysis. The outcome of the results from these multidisciplinary analyses were integrated into a 3D geomechanical model using the 3D seismic elastic inversion and pore pressure cube. This 3D model was used to evaluate the drilling risks, optimize the drilling operations, and plan for the new well trajectories for the field development.

In situ stress directions were inferred from the drilling induced tensile fractures observed on the borehole images. In this highly complex tectonic area, stress rotations with depth were identified from shallow (~2,000 ft) to deep (~18,000 ft) as maximum principal horizontal stress (S_{Hmax}) trends NE-SW and S_{Hmax} NW-SE — in the reservoir. At reservoir level, the stress direction also changes laterally, therefore, two dominant S_{Hmax} trends, NW-SE and WNW-ESE, were identified in the reservoir. These two trends have a close relationship with major faults and are aligned with the fault lineaments identified on the 3D seismic. The natural fractures identified in the reservoir are also aligned with these faults.

Geomechanics facies were identified by integrating the rock mechanical properties, sonic anisotropic analysis and the fracture interpretation from borehole images. These results demonstrate the presence of a particular facies in the wells, which encountered severe drilling issues, e.g., total loss circulation. This particular facie is trackable in the field to circumvent new well placement; it is characterized by high anisotropy and the presence of open natural fractures.

INTRODUCTION

Understanding and mapping stress and natural fractures can be very important to enhance the drilling efficiency. Generally, stress orientations and fractures can be interpreted from borehole images, sonic logs, and seismic data[1]. Detailed stress mapping in this study describes the in situ stress rotations and their implications on the mechanical behavior of the natural fractures in a highly complex tectonic area.

This study presents the integrated results of drilling data,

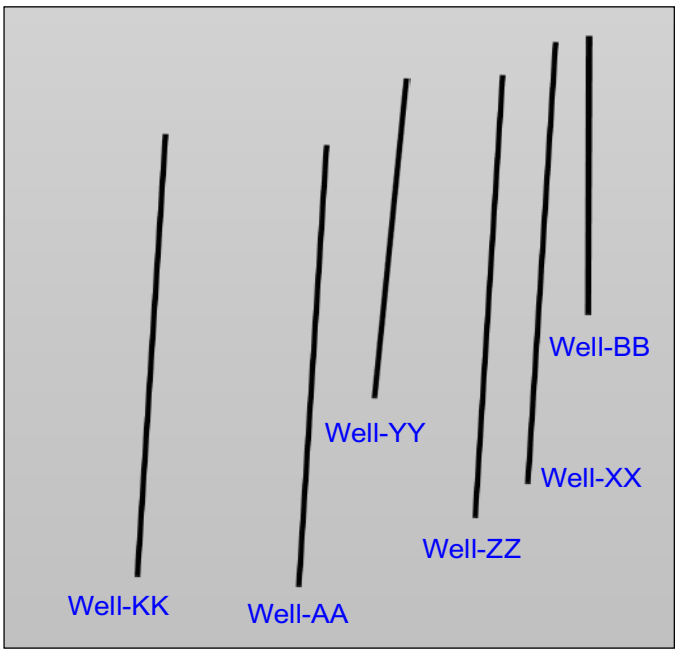

Fig. 1. Structural surface for the Zone D (reservoir) and well locations.

borehole images, dipole sonic, and borehole seismic, core triaxial tests, 1D geomechanical modeling, critical stressed fractures and 3D seismic attribute analysis. These analyses were integrated into a 3D mechanical earth model (MEM) to characterize in situ stress rotations at pre-production conditions for various zones (A, B, C, and D) in the carbonate reservoir, Saudi Arabia.

Rock mechanical properties and rock physics analysis were performed for 11 wells distributed along Zone D, Fig. 1. Seismic elastic inversion was used to estimate the rock mechanical properties for the 3D geological model, showing a consistent match with the mechanical properties estimated based on the well logs. A pore pressure cube was derived from seismic interval velocity analysis, assuming loading conditions using compaction trend lines and available direct pore pressure measurements from available wells and constrained by the mud weight used in

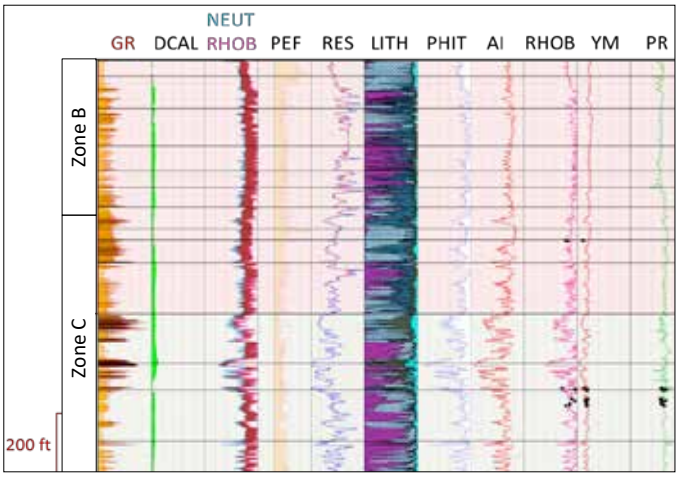

Fig. 2. Ultrasonic core test data were used to calibrate the dynamic rock properties derived from sonic and density logs from Well-XX.

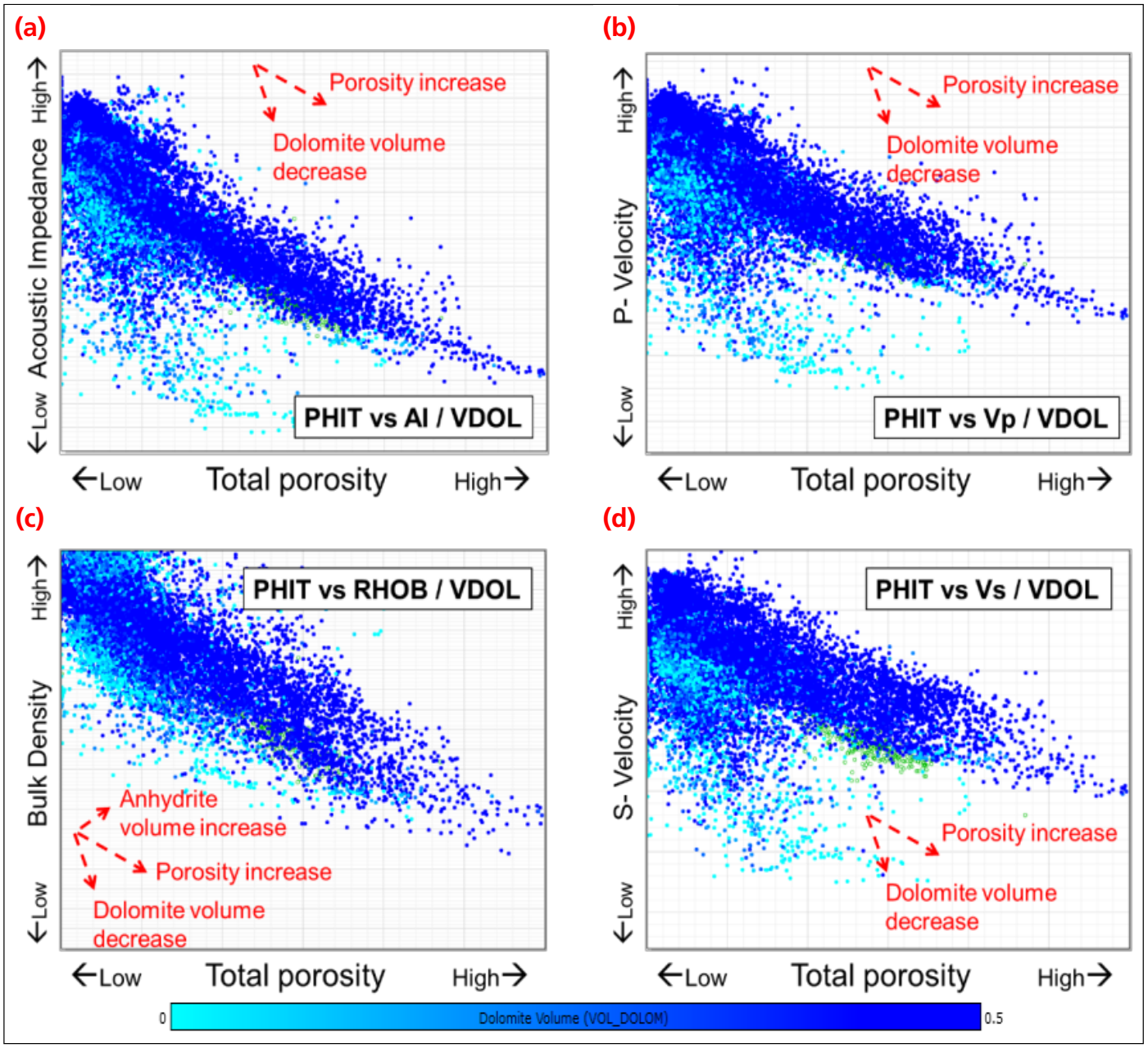

Fig. 3. Quality control: Cross-plots were used to analyze the trends and relationship between different rock parameters with respect to the total porosity (PHIT).

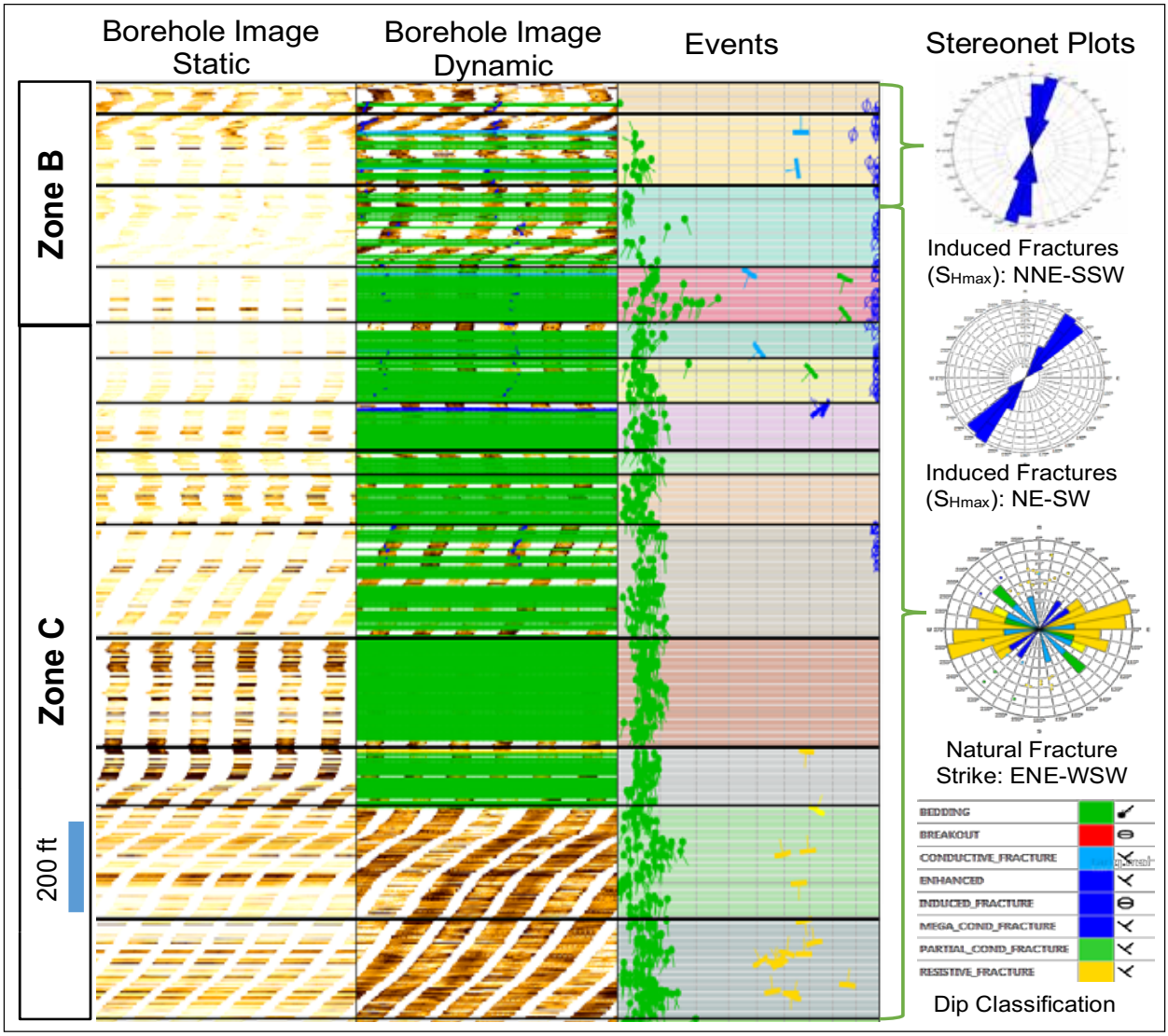

Fig. 4. Fracture characterization composite showing the main features identified from the borehole images.

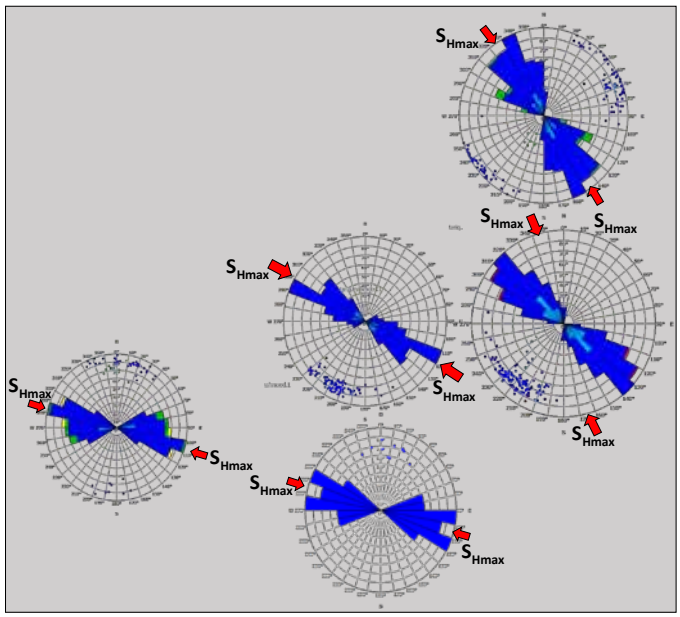

Fig. 5. Natural fractures and stress distributions in the reservoir (Zone D).

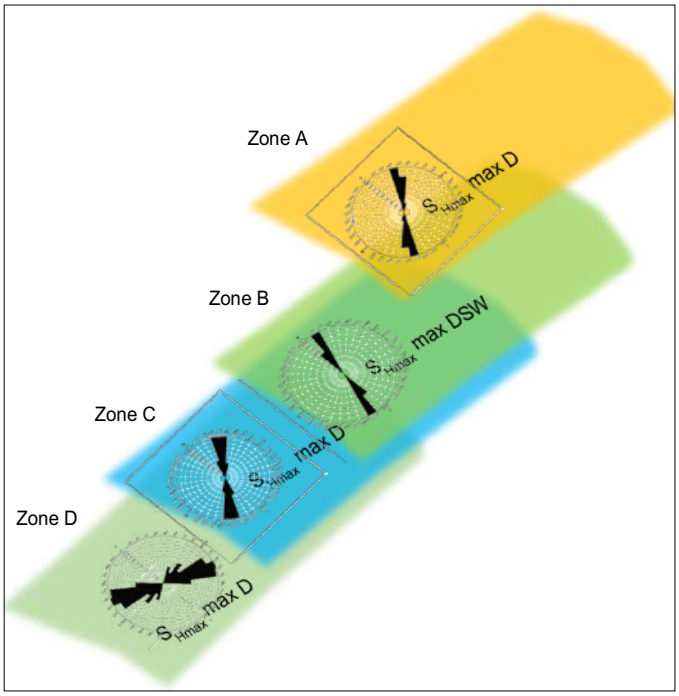

Fig. 6. The S_{Hmax} rotation identified within Zones A to D — from a shallow section of the reservoir to a deeper section.

drilling these wells. In this study, a critical stressed fracture analysis technique was used to determine the relationship between the in situ state of stress and the fracture geometry. These critically stressed features were the main root cause of loss circulation, causing the major drilling troubles.

The present day stress regime identified in our analysis is categorized as strike-slip-faulting regime for which the maximum principal horizontal stress (S_{Hmax}) is the largest principal stress, i.e., $S_{Hmax} \geq S_v \geq S_{hmin}$. Our study covers a large vertical section with depths ranging from 500 ft to 17,000 ft. Detailed wellbore image logs analysis was conducted to differentiate between natural fractures and drilling induced tensile fractures[2]. In situ stress direction was inferred from drilling induced tensile fractures, which propagate parallel to the borehole axis — 180° apart. We observe that the S_{Hmax} orientation rotates with depth (~500 ft) to the deep (~17,000 ft) section, varying from Zone A S_{Hmax} NE-SW, Zone B S_{Hmax} NNE-SSW, Zone C S_{Hmax} NE-SW, and Zone D S_{Hmax} NW-SE.

ROCK PHYSICS

Understanding the behavior of elastic properties to get the realistic discrimination on lithology, porosity and mechanical properties is important to minimize the pitfalls in the interpretation and geomechanical modeling in carbonates. Carbonate rocks are known for their complexities in pore geometry, network and mineralogy. These complexities are a major cause of the highly scattered porosity velocity relationship solvable by rock physics models.

Rock physics models are mathematical equations based on physical principles to generate P- and S- velocities based on rock structure, composition and properties. By setting some of the parameters, say dolomite and limestone bulk and shear modulus, the equations can be solved to predict velocities in missing data intervals. The main advantage of this approach is that all relations between elastic properties and rock quality are preserved.

Development of robust and accurate rock physics models in carbonates is a crucial step toward successful geomechanical applications. The rock physics model is focused on predicting dynamic Vp and Vs as accurate as possible, which is suitable for further mechanical modeling[3].

A tangential shear factor was used to obtain an optimal match with observed Vp/Vs ratios, since this approach is known to over predict shear wave velocities by neglecting rotational freedom and slip at grain contacts. Vp and Vs are functions of porosity, mineralogy, differential pressure and saturation[4]. The setup of the input parameters was completed iteratively to find the realistic mineral properties to be used for this data set. This can be thought of as inverting for solid minerals elasticity for the data set, assuming that all other properties are known, and that the model is correct. Then, the calculated Vp and Vs were calibrated on dynamic mechanical properties derived from core analysis to obtain the best fit between all available data. Dynamic rock properties were obtained from an ultrasonic core test and were used to calibrate the dynamic Poisson's ratio and dynamic Young's modulus for Well-XX, Fig. 2.

The cross-plotting of elastic parameters is a useful tool for quick interpretation of elastic and mechanical properties' behavior and anomalies. It is observed that the effect of different lithology and porosity is separated in acoustic impedance, velocity and density domains, Fig. 3.

FRACTURE CHARACTERIZATION

Natural fractures were characterized and differentiated from drilling induced tensile fractures based on the criteria by using borehole images[2]. These natural fractures in the reservoir have two dominant trends NW-SE and WNW-ESE, and are oriented with the major lineaments identified on the 3D seismic. One set of these fractures is sub-parallel to the S_{Hmax} direction, thereby placing these candidates at an optimal position to be critically stressed under the present-day stress conditions.

Dip interpretation based on the borehole image logs from the wells in the studied area provides quantification of fracture strike orientations and fractures dip and azimuth distributions, Fig. 4.

STRESS ROTATIONS

In Situ Stress Analysis

In this study, drilling induced tensile fractures were used to constrain the S_{Hmax} direction. The natural fractures in the reservoir (Zone D) have two dominant trends NW-SE and WNW-ESE, Fig. 5. Figure 6 illustrates the S_{Hmax} rotation identified within Zones A to D — from a shallow section of the reservoir to a deeper section; however, the S_{Hmax} direction supplements additional complications as it is not consistent at the reservoir level. We observed two dominant orientations, NNW-SSE and WNW-ESE, of S_{Hmax} at the reservoir level, Fig. 7. The natural

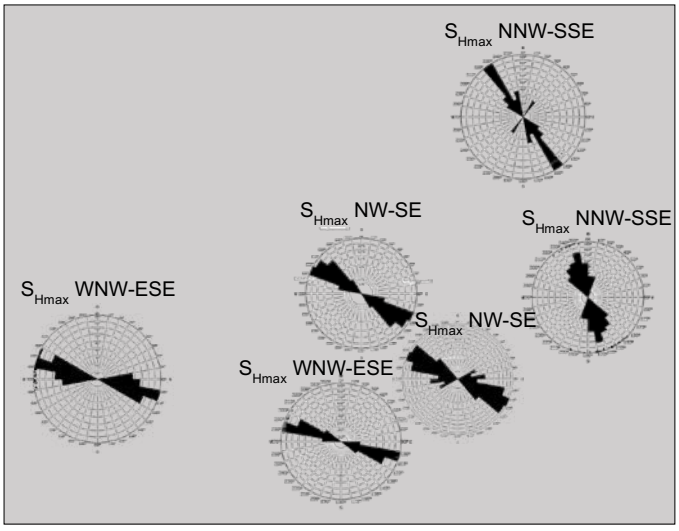

Fig. 7. The S_{Hmax} directions showing lateral variations, from NNW-SSE and WNW-ESE, for the reservoir section.

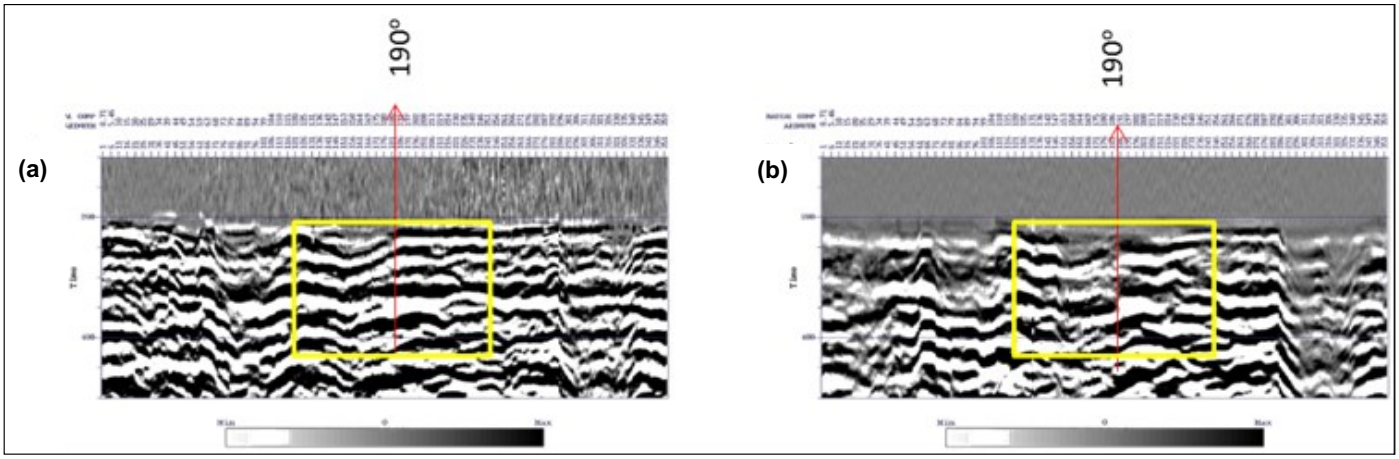

Fig. 8. Azimuthal common receiver gathers, (a) radial, and (b) transverse component showing the shear downgoing wavefield in Zone B.

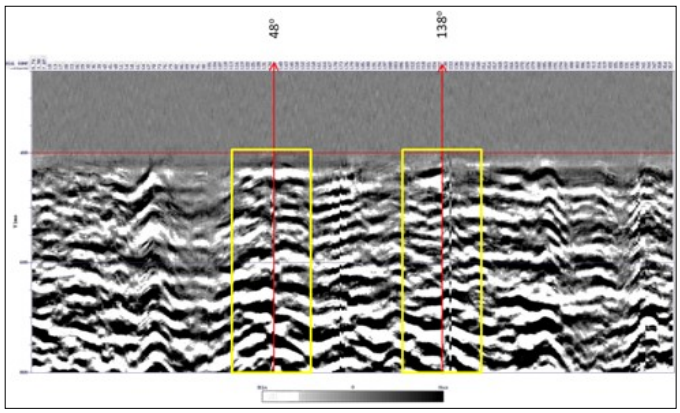

Fig. 9. Azimuthal common receiver gathers, (transverse component) showing the shear downgoing wavefield in Zone C.

fractures trends generally follow the same orientation trend as that of the S_{Hmax} direction.

Walkaround Vertical Seismic Profile (VSP)

In situ stress orientation was also determined for the walkaround vertical seismic profile (VSP), which was consistent with results from image log analysis as discussed in the previous section. The walkaround VSP was designed for Well-JJ, using existing 3D surface seismic data and information from neighboring wells. The objectives were to measure the traveltime variation within the target intervals, measure the polarization of the downgoing P-waves, and measure the shear wave splitting of the downgoing and upgoing converted shear waves (PS) through the intervals between the top of Zone B and the top of the Zone D. After modeling, it was decided to use a source offset of 1,700 m. An air gun array source was used, where 120 receiver levels were recorded with a receiver array spacing of 50 ft. The shot spacing was approximately every 25 m and a total of 395 shots were acquired.

Horizontal rotation, gain and a spherical divergence correction were applied to the raw data. A careful wavefield separation was performed to isolate the downgoing and upgoing shear wavefields in the radial and transverse components. Common receiver gathers were then created to verify polarity reversals and time delays between the fast and slow shear waves to identify the naturally fast polarization directions. Azimuthal slowness variation of the P- and S-waves were evaluated. To estimate the anisotropic axis related to stress induced anisotropy in Zones B and C, a joint analysis of shear wave splitting and azimuthal traveltime variations was performed. Subsequently, as the VSP receivers were not available in Zone D, the azimuthal traveltime variations of PS reflections ahead of the bit were used to identify the anisotropic axes.

The shear anisotropy detected by the walkaround VSP shows directions NNE-SSW for Zone B, NE-SW for Zone C, and NW-SE for Zone D. Figure 8 shows the azimuthal common receiver gathers, radial and transverse components, of the shear downgoing wavefield in Zone B. Figure 9 shows the polarity flips observed in Zone C — the transverse component at 48° and 138°. These polarity flips observed in Zones B and C agreed with the directions of the anisotropic axes found using analysis of the azimuthal slowness. Figure 10 shows an

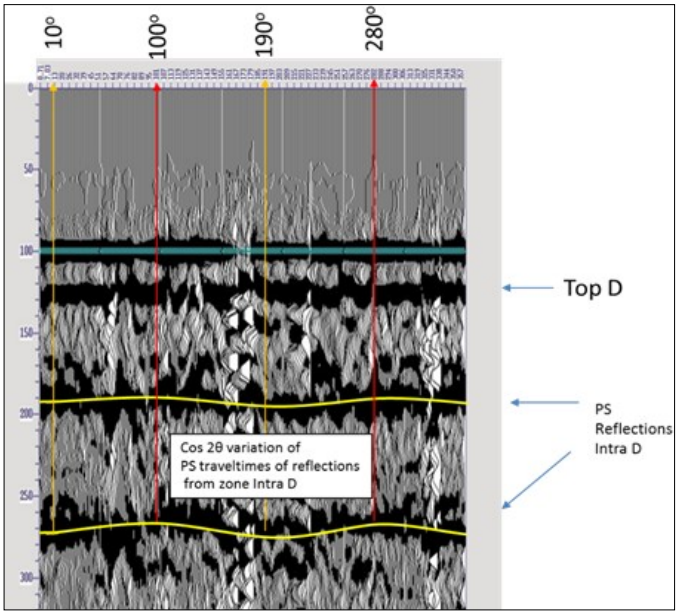

Fig. 10. Azimuthal common receiver gathers, (transverse component) showing the PS upgoing wavefield in Zone D.

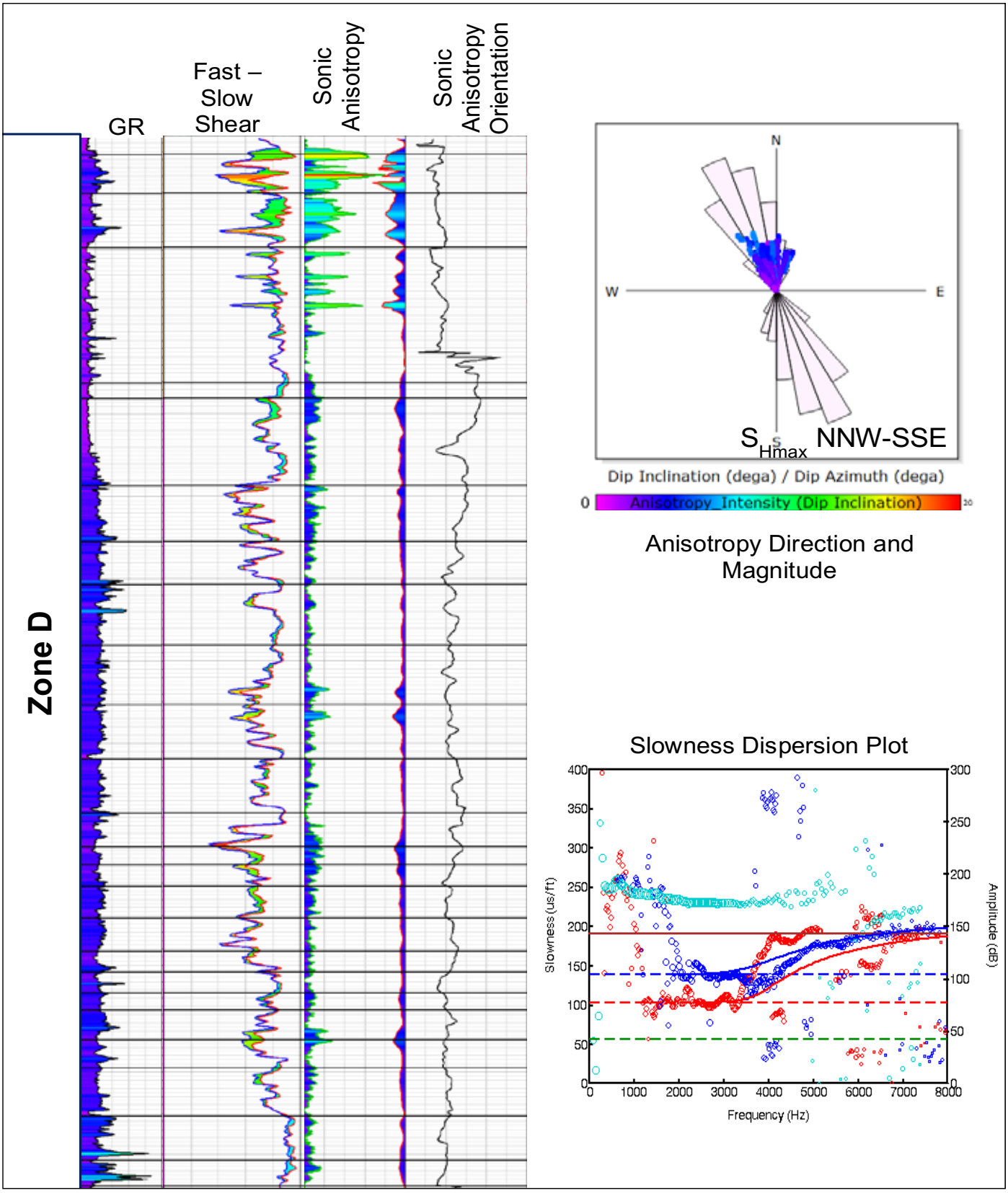

Fig. 11. Sonic acoustic anisotropy induced by stress, indicating the maximum stress orientation.

azimuthal common receiver gather of the upcoming PS wavefield aligned on the P-wave's first arrivals. Cos 2θ variation is observed for the reflections intra-Zone D. The fast shear direction is indicated by the red arrows.

Sonic Acoustic Anisotropy

To understand and integrate the type of anisotropy in this field, we acquire acoustic anisotropy logs in two wells, Well-XX and Well-YY, in the reservoir zone. Azimuthal shear anisotropy

analysis is a powerful tool to identify the type of anisotropy, whether it is due to stress or fractures[5]. Our analysis shows the type of anisotropy identified in one well is stress induced, Fig. 11. These results are consistent with the borehole image and walkaround VSP analysis discussed in previous sections.

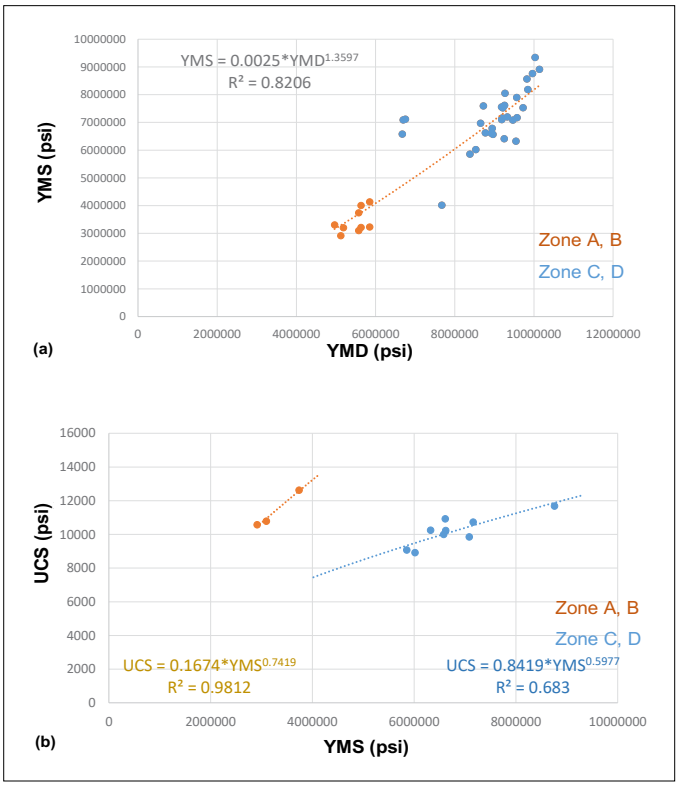

Fig. 12. Mechanical correlations derivate from a triaxial rock mechanical test.

IN SITU STRESS MODEL

The wireline logs from 11 wells were used to estimate the stress profile magnitude. Along the wells, mechanical correlation was derived from multistage triaxial rock mechanical tests, performed in Zones B and C.

Rock Mechanical Properties

The dynamic Young's modulus, shear modulus, bulk modulus and the Poisson's ratio of the rock were generated from the compressional sonic, shear sonic and density logs. The static properties' empirical correlations from a triaxial test were also estimated. These correlations were estimated with regression from the wells with available information.

Laboratory measurements provide the possibility to constrain a range of physical rock properties, including uniaxial compressive strength (UCS), coefficient of internal friction, Young's modulus, and Poisson's ratio. Correlations between dynamic and static rock properties were derived from rock mechanical core plug tests. Static rock properties and rock strength properties were estimated from dynamic properties, showing significant variation in Young's modulus between Zones A, B, C, and D that were found changing from 3 Mpsi to 9 Mpsi. Figures 12a and 12b illustrate the variations between the triaxial rock mechanical properties.

Pore Pressure

Pore pressure profiles were modeled using compaction trend lines in the velocity logs assuming a loading process. It was

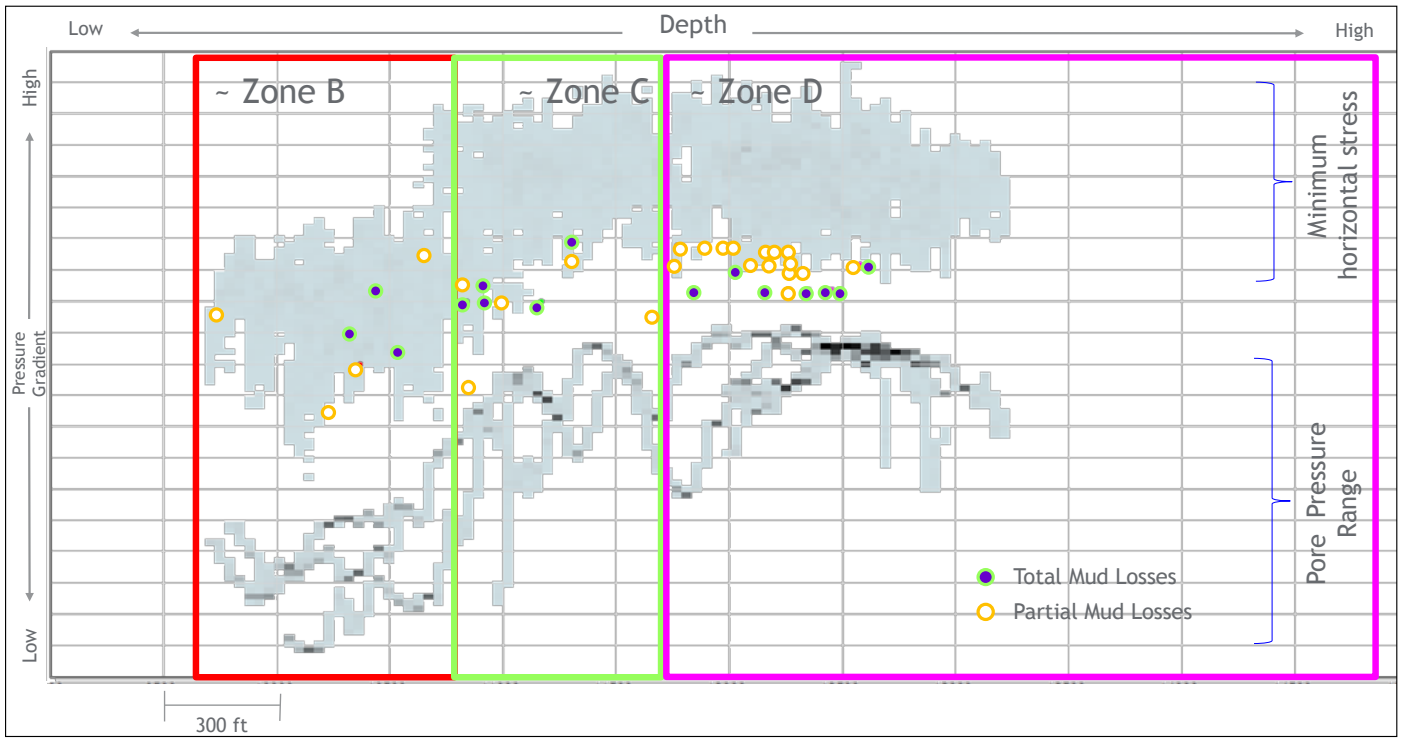

Fig. 13. Pore pressure and S_{Hmin} gradient associated with the wells reported with mud losses.

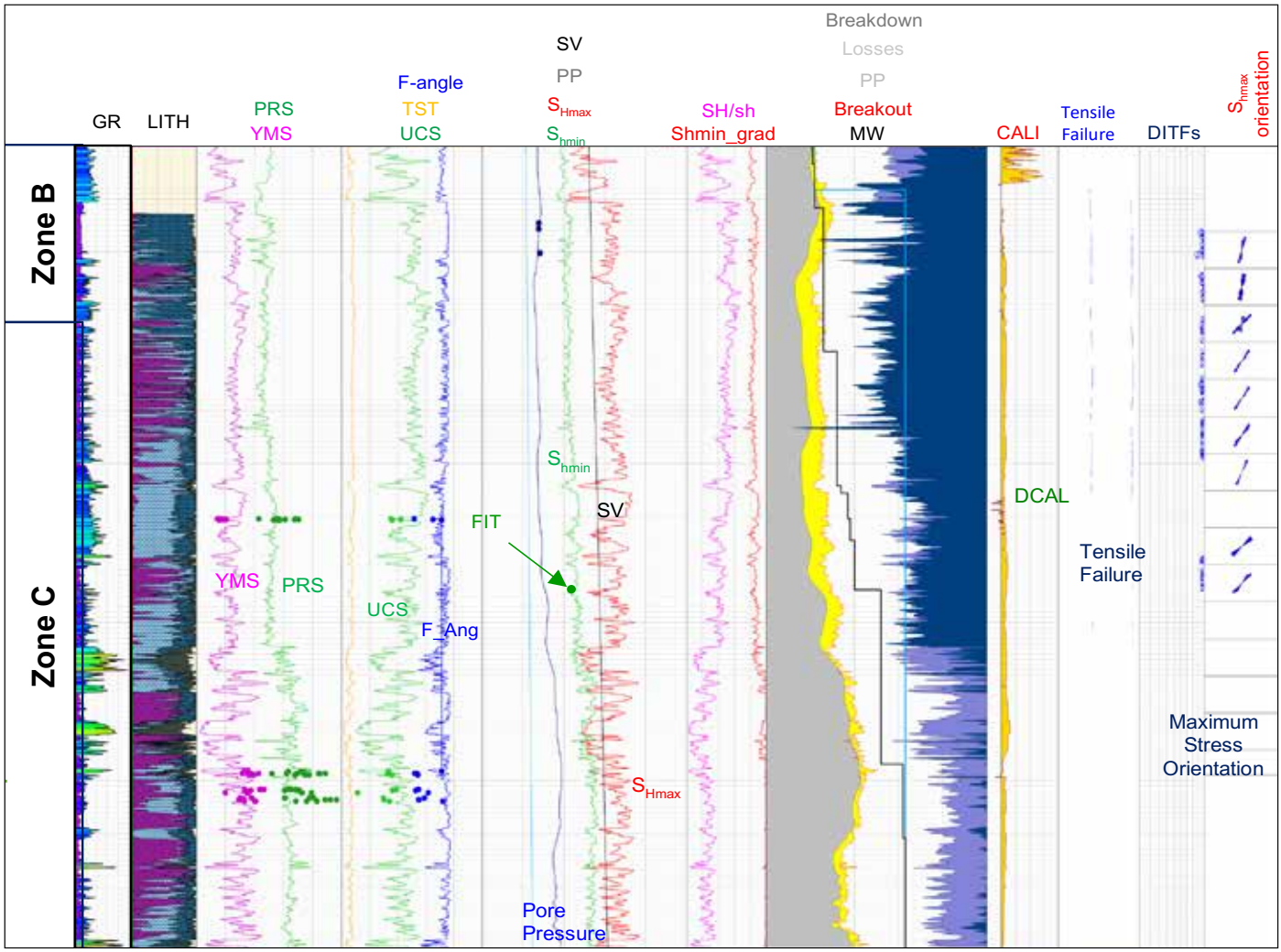

Fig. 14. Composite plot for Well-KK, showing the main stress profiles and wellbore stability from the 1D geomechanics process. Track 1: Stratigraphy through the reservoir section. Track 2: Gamma ray. Track 3: Mineralogical model estimated from petrophysics interpretation. Track 4: Static rock properties with Poisson's ratio (light green) and Young's modulus (pink). Track 5: Rock strength properties with unconfined compressional strength (light green), friction angle (dark blue) and tensile strength (orange). Track 6: Calculated stress profiles with pore pressure (dark blue), S_{hmin} (green), S_{Hmax} (red), S_v (black), FIT (green dot) and modular dynamic tester (black dot). Track 7: Ratio between S_{Hmax}/S_{hmin} (red) and Shmin gradient (pink). Track 8: Calculation of the stable mud weight window. Limits are calculated for kicks (grey), breakouts (red), mud losses (blue) and formation breakdown (purple), and the drilling mud weight (dark yellow line). Track 9: Caliper logs. Track 10: Tensile Failure. Track 11: Drilling induced tensile fractures. Track 12: Maximum stress orientation.

observed that the pore pressure increases with depth from 0.5 psi/ft, reaching up to 0.7 psi/ft. The computed pore pressure in Zones B and D were calibrated with direct measurements. Figure 13 illustrates the pore pressure results.

Stress Magnitude

The overburden (vertical) stress was calculated by using the density logs, which shows an average gradient of approximately ~1.15 psi/ft.

The minimum stress magnitude was estimated using poroelastic equations and available leakoff test and formation integrity test (FIT) recorded in the field. The analysis shows a consistent change from 0.8 psi/ft for Zones A and B, to 0.85 psi/ft for the Zones C and D.

The S_{Hmax} was estimated using the poroelastic model, constrained by the wellbore stability model and drilling events, also used were the borehole image interpretation (drilling induced tensile fractures and borehole breakouts) and the average value estimated was around ~1.3 psi/ft to ~1.4 psi/ft. Figure 14 illustrates the geomechanical modeling results.

Geomechanics Facies, Acoustic Anisotropy and Fracture Detection

Geomechanical facies were computed as a pattern model using the elastic rock properties and stress magnitude profiles, making mathematical combinations between the variables classifying the formation into mechanical layering "facies." Geomechanics facies were computed for five wells using the rock mechanical properties, computing all the possible scenarios between the elastic properties. The results from those combinations were compared with the sonic acoustic anisotropy, showing that only one particular facie, (red flag) has a good relation with the high anisotropy. This high anisotropy was identified as "intrinsic" caused by open natural fractures[6]. These natural fractures

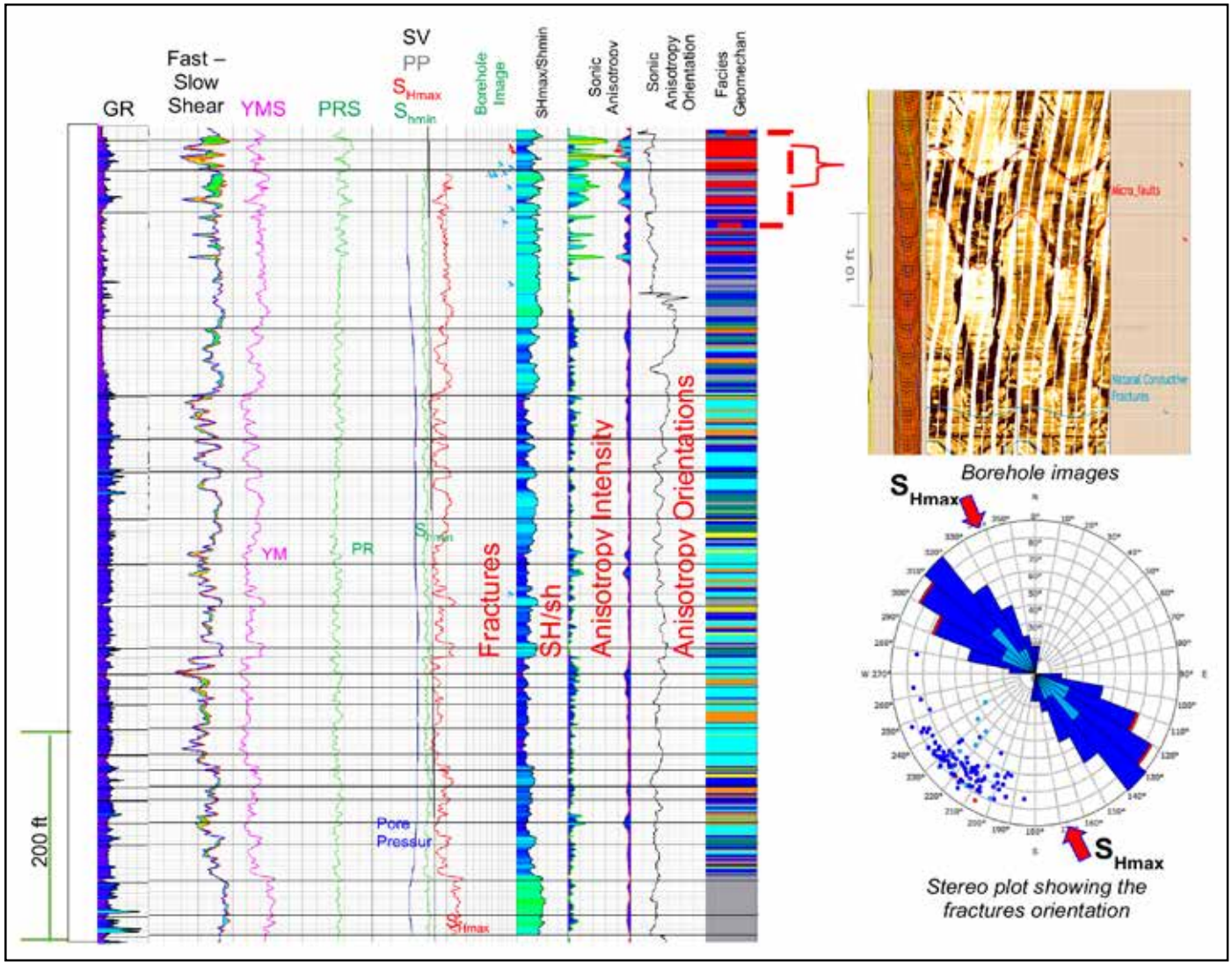

Fig. 15. Geomechanics facies and acoustic anisotropy showing the red flag for Zone D associated with a high acoustic anisotropy response for Well-XX.

were also observed on the borehole images, Fig. 15. This well, Well-XX, encountered 100% mud losses over this interval while drilling.

The same geomechanics facies classification was applied to the other wells, Well-YY, Well-ZZ, Well-AA, and Well-BB; identifying with the red flag only to Well-YY. Well-YY has a few natural fractures interpreted over the red flag facies, also showing high anisotropy over this facies. The wells don't show "intrinsic" anisotropy induced by open natural fractures. No drilling issues were encountered in these wells while drilling. Figure 16 illustrates the geomechanics facies correlations for five wells.

3D MEM

The seismic elastic inversion was used to estimate the dynamic and static properties. Static Young's modulus and static Poisson's ratio were estimated using the correlations defined from the 1D MEM. Additionally, unconfined compressional strength was estimated using different equations for Zones A, B, C, and D, due to the high heterogeneities between the carbonate units.

The compaction line defined in the 1D MEM was applied to the interval velocity from the seismic data, to estimate the pore pressure for the entire Zones A, B, C, and D. The pore pressure derived from velocity analysis was compared with mud weight used to drill the wells and direct pore pressure measurements, Fig. 17.

The horizontal stresses predicted from the 3D geomechanics model were compared with the 1D MEM results, showing a good correlation between the S_{Hmax}, S_{hmin} and vertical stress, however, a 3D model was unable to resolve high resolution from the 1D MEM, Fig. 18. A wellbore stability model was created based on the 3D stress prediction and compared with the 1D MEM, Fig. 19.

Two scenarios (undisturbed and disturbed) were considered for Zone D in the geomechanics simulations.

Undisturbed Scenario

This scenario assumes the model without any lineaments or faults/fractures that can perturb the stress orientation and magnitude. This scenario sets the S_{Hmax} orientation to NW-SE and remains constant for the whole model, Fig. 20.

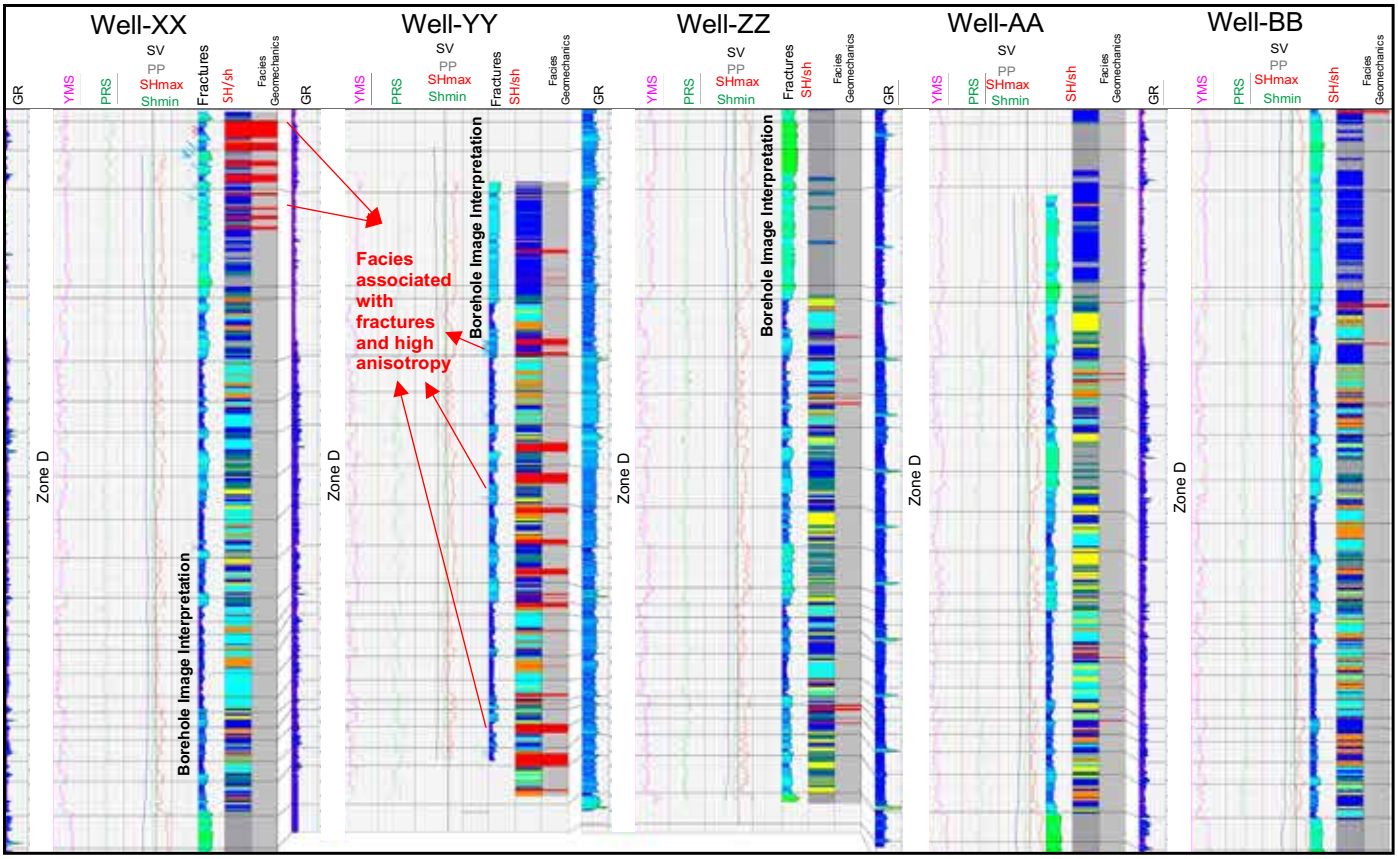

Fig. 16. Geomechanics facies correlation showing the red flag only, presented in the five wells rported with natural fractures and associated mud losses.

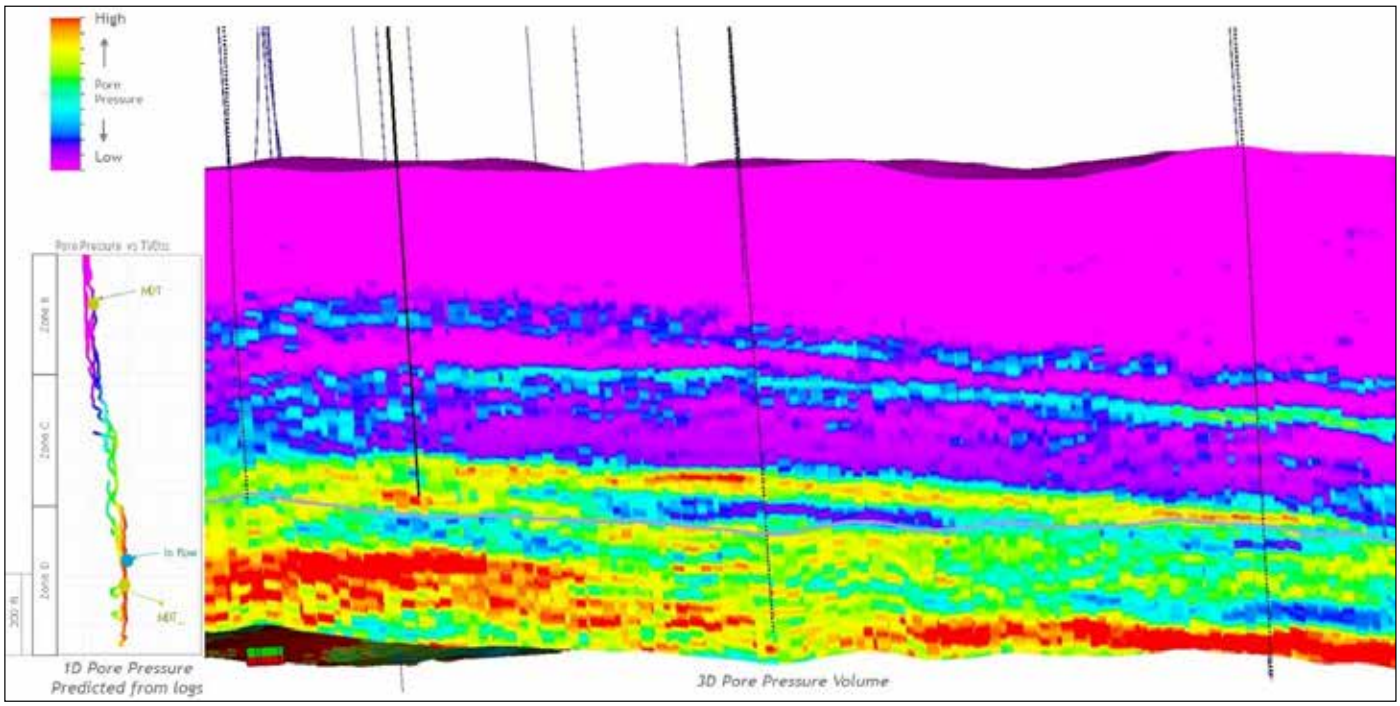

Fig. 17. Comparison between the pore pressure from the 1D MEM and interval velocity.

Disturbed Scenario

In Zone D, the S_{Hmax} orientation was identified with significant lateral variations, Fig. 21. These stress directions were mainly aligned with 3D seismic lineaments. In our 3D geomechanical modeling, the seismic lineaments were defined as an inflexion point for the stress rotations to match the maximum stress tensor predictions, and interpreted from borehole images.

NORMAL AND SHEAR STIFFNESS ANALYSIS

The main objective is to identify critically stressed fractures[7],

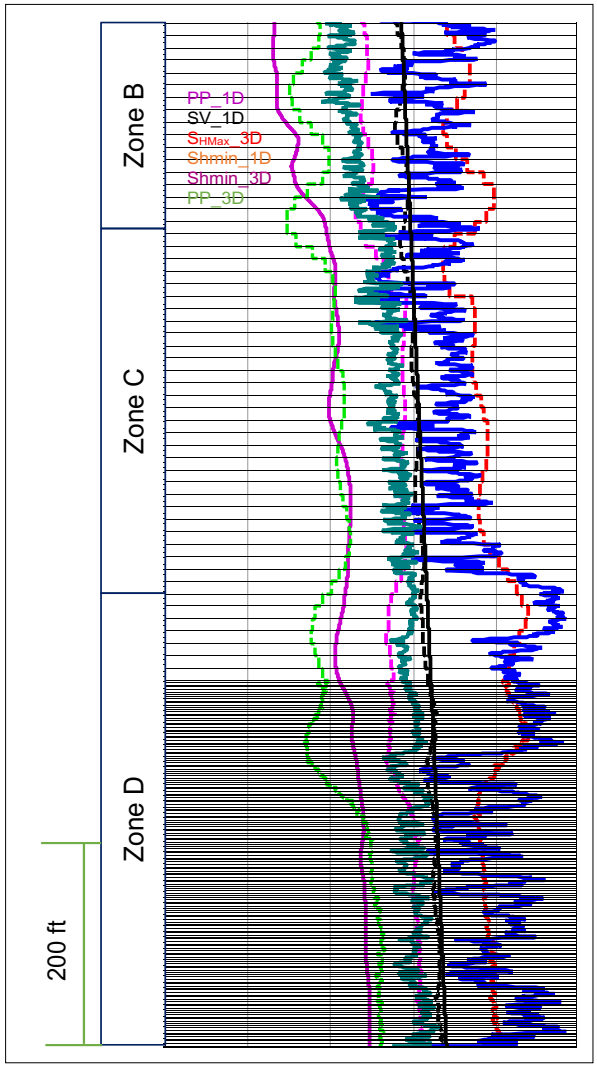

Fig. 18. Comparison between the stress profiles predicted from the 1D MEM and 3D MEM.

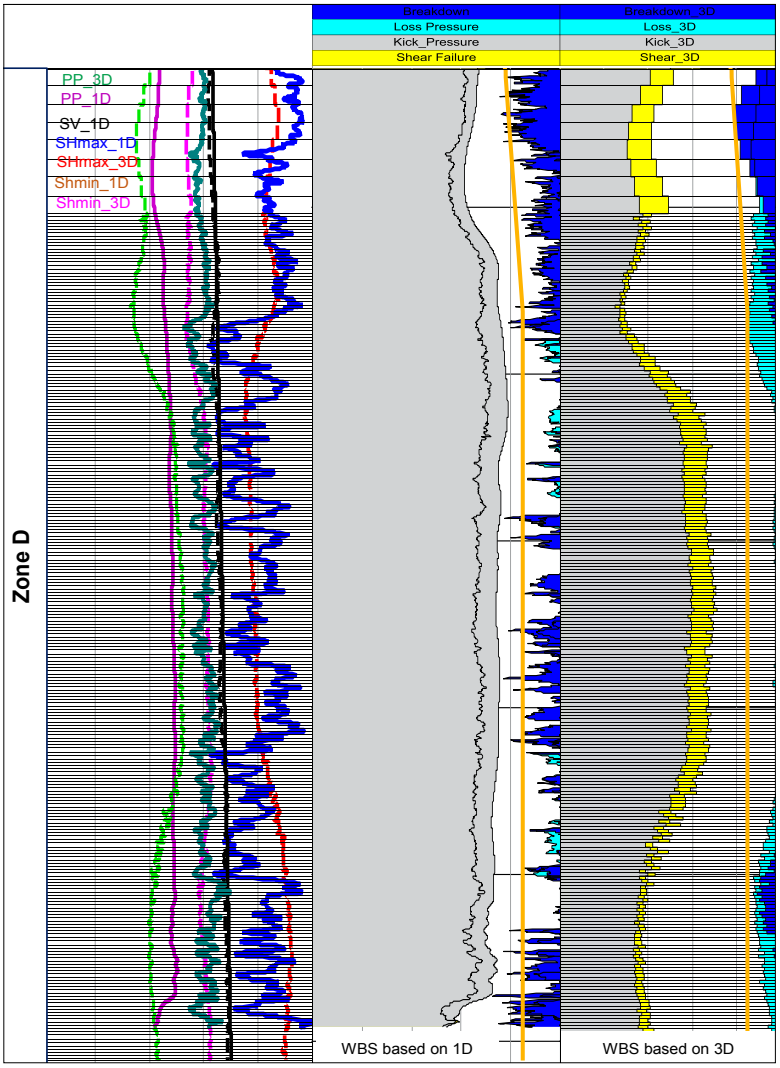

Fig. 19. Comparison between the wellbore stability profiles predicted from the 1D MEM and 3D MEM.

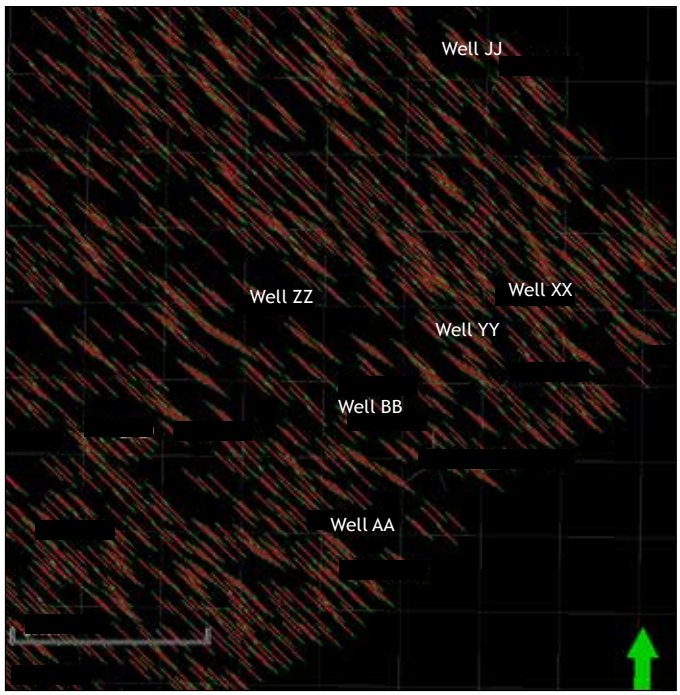

Fig. 20. Undisturbed model keeping a constant S_{Hmax} direction.

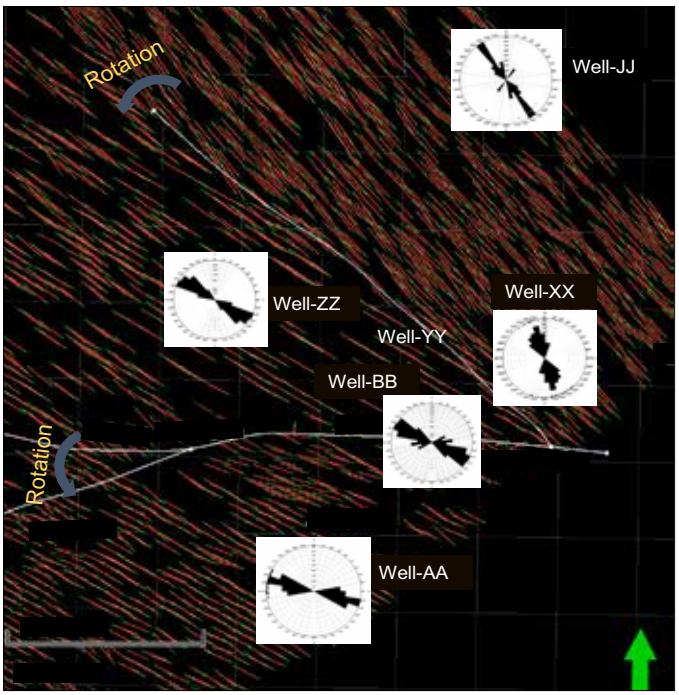

Fig. 21. Disturbed S_{Hmax} and borehole image interpretation.

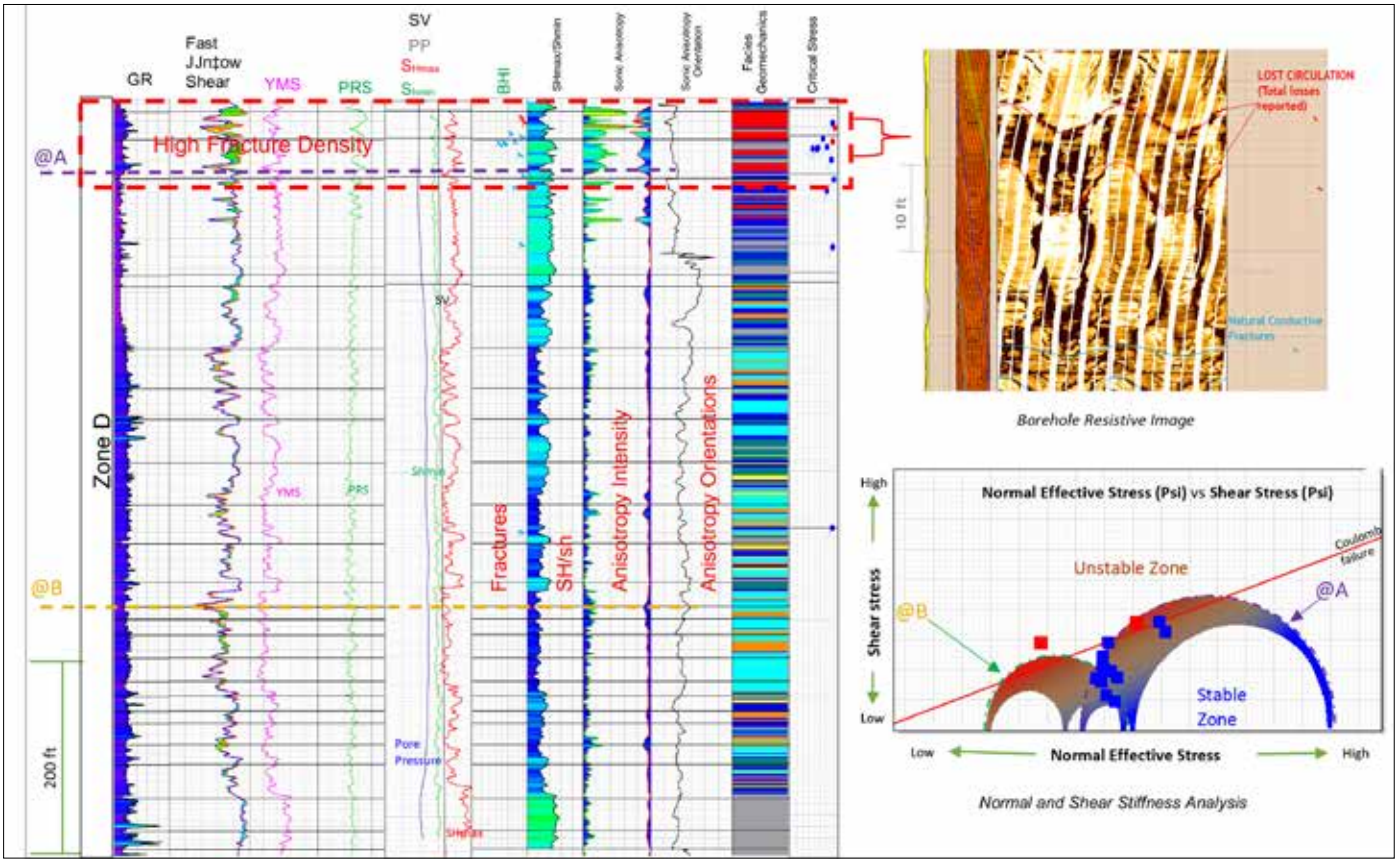

Fig. 22. Normal and shear stiffness analysis for Well-XX showing a critical state of some fractures associated with mud losses, high anisotropy and geomechanics facies.

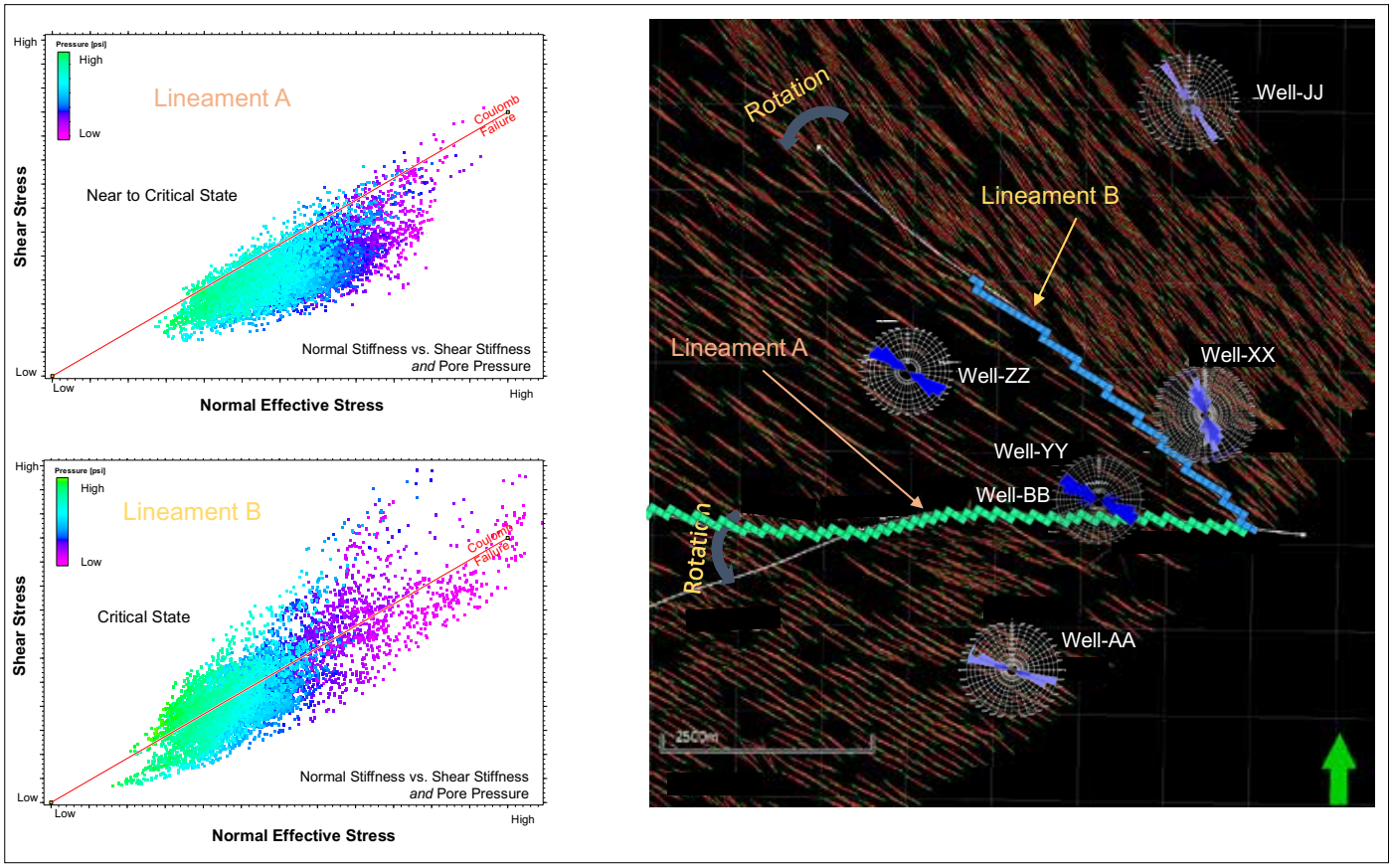

Fig. 23. Normal and shear stiffness estimated for the alignments identified from a 3D seismic analysis.

which are more likely to be permeable, and therefore, more likely to control fluid flow within a reservoir. In this technique, permeable fracture predictions are made by using the "Mohr-Coulomb Failure Criterion." This is a linear relationship between the shear stress and the effective normal stress acting on a fracture or fault plane. Sliding will occur when the ratio of shear to effective normal stress is equal or greater than the friction angle. We are using this technique to determine the relationship between the in situ state of stress and fracture geometry to identify the critically stressed fractures. Fractures used in this technique are mainly derived from the borehole images. These fractures also are located over the red flag geomechanics facies and high acoustic anisotropy in certain parts of the field. It was concluded that these fractures are the main reason for the mud losses encountered during drilling. Figure 22 illustrates the critical stress analysis, geomechanical facies and fracture identified from borehole images.

Additionally, using the 3D geomechanical model, the normal and shear stiffness analysis were estimated into two main lineaments identified by 3D seismic attribute analysis. The results show that the lineaments toward the direction of S-SE (blue path) are probably under a more critical state than the lineaments toward the direction of E-W (green path), Fig. 23.

RESULTS AND DISCUSSIONS

1. The stress regime is characterized by strike-slip-faulting, for which the S_{Hmax} is the largest principal stress, i.e., $S_{Hmax} > S_v > S_{hmin}$. The field is associated with complex tectonic events, possibly related to salt movements in the deeper sections.
2. The calibrated stress model was established based on the poroelastic equations, fracture close pressure, core data, wellbore stability model and drilling events showing an average anisotropy ratio of approximately 1.62:1.64 — maximum principal stress magnitude/minimum principal stress magnitude.
3. Stress rotations were identified from borehole images, acoustic sonic anisotropy and VSP walkaround showing consistent results.
4. In the reservoir, the lateral changes in the stress directions are mainly related to lineaments and/or faults observed on the 3D seismic analysis.
5. The critically stressed fractures have a strong relationship with mud losses reported in the respective wells.
6. High anisotropy induced by stress and natural fractures is related with the geomechanics facies, and can be useful to predict natural fractures away from the wellbores.
7. The walkaround VSP confirmed the effect of fractures and stress induced anisotropy in the seismic data.

ACKNOWLEDGMENTS

The authors would like to thank the management of Saudi Aramco for their support and permission to publish this article.

REFERENCES

1. Tyiasning, S. and Cooke, D.: "Anisotropy Signatures in the Cooper Basin of Australia: Stress vs. Fractures," *Interpretation*, Vol. 4, Issue 2, May 2016, pp. SE51-SE61.
2. Mahmood, T.: "Methodology to Discriminate Natural vs. Drilling Induced Tensile Fractures Using Borehole Images — Critical for Wellbore Failure Analysis and Natural Fracture Characterization," paper 90254, presented at the 12th Middle East Geosciences Conference and Exhibition, Manama, Kingdom of Bahrain, March 7-10, 2016.
3. Xu, S. and White, R.E.: "A New Velocity Model for Clay-Sand Mixtures," *Geophysical Prospecting*, Vol. 43, Issue 1, January 1995, pp. 91-118.
4. Xu, S., Chen, G., Zhu, Y., Zhang, J., et al.: "Carbonate Rock Physics: Analytical Models and Validations Using Computational Approaches and Lab/Log Measurements," IPTC paper 11308, presented at the International Petroleum Technology Conference, Dubai, UAE, December 4-6, 2007.
5. Ostadhassan, M., Zeng, Z. and Jabbari, H.: "Using Advanced Acoustic Data to Determine Stress State Around Wellbore," ARMA paper 11-319, presented at the 45th U.S. Rock Mechanics/Geomechanics Symposium, San Francisco, California, June 26-29, 2011.
6. Velez, E.I., Vasquez, J., Frydman, M., Janampa, H., et al.: "Novel Approach for Fracture Characterization in a Metamorphic Reservoir," SPE paper 138965, presented at the SPE Latin American and Caribbean Petroleum Engineering Conference, Lima, Peru, December 1-3, 2010.
7. Zoback, M.D.: *Reservoir Geomechanics*, Cambridge University Press, Cambridge, 2007, 461 p.

BIOGRAPHIES

Dr. Tariq Mahmood joined Saudi Aramco in 2008 and currently works in the Gas Reservoir Characterization Department as a Geological Consultant. He began his career in 1996, working in Perth, Australia, specializing in fractures/faults characterization from borehole images. Tariq has provided consultancies to major oil companies in the Asia Pacific region and Australia, including Shell Brunei, Petronas, Chevron, Santos, Apache, Woodside, etc. Since joining Saudi Aramco, he has worked on many interesting projects addressing a variety of problems in both offshore and onshore fields.

Tariq is a member of the American Association of Petroleum Geologists (AAPG), the European Association of Geoscientists and Engineers (EAGE), and the Dhahran Geosciences Society (DGS). He is the coauthor of three patents.

Tariq received his Ph.D. degree in Geology from the University of Adelaide, Adelaide, South Australia, Australia, in 1996. Based on his Ph.D. research, an atlas on the "3D Analogue Modeling of Extensional Fault Systems plus Field Applications" was published by the University of Adelaide. Tariq was the recipient of the Harold Rhoda Scholarship during his studies in Australia.

Otto E. Meza Carmargo joined Saudi Aramco in 2014 as a Geologist Engineer working in the Exploration Technical Services Department. He has 10 years of experience in the oil industry, and prior to joining Saudi Aramco, he worked in a variety of geological positions across the Middle East region, Brazil, Peru and the U.K. Otto's experience includes several aspects of reservoir characterization and integrated geomechanics modeling for conventional and unconventional reservoirs.

He received his B.S. degree in Geological Engineering from the University of San Marcos, Lima, Peru.

Ali H. Al-Gawas is a Reservoir Geophysicist with Saudi Aramco's Ghawar Jurassic Team of the Abqaiq/Ghawar Fields Division, in the Reservoir Characterization Department (RCD). In 2007, he joined Saudi Aramco, where he worked in seismic data acquisition, processing, and interpretation. Then, in 2010, Ali began work as a Gas Reservoir Geophysicist. His research interest includes rock physics, fractures, and interpreting seismic data.

In 2007, Ali received his B.S. degree in Geophysics from Boise State University, Boise, ID, and in 2015, he received his M.S. degree in Geophysics from King Fahd University of Petroleum and Minerals (KFUPM), Dhahran, Saudi Arabia.

Khalid A. Al-Hawas is a Reservoir Geophysical Consultant and a Team Leader in the Abqaiq/Ghawar Fields Division with Saudi Aramco's Southern Reservoir Characterization Department (SRCD). His extensive experience began in 1994, when Khalid began working on structural and fault interpretation using seismic properties and attributes. In 1999, Khalid further expanded his experience on seismic attribute analysis when he went on a one year assignment with Chevron's research group, based in La Habra, CA.

Then, in 2000, Khalid returned to SRCD and started applying and promoting the use of azimuthal seismic anisotropy for fracture detection integrating multiscale, multi-tool data within Saudi Aramco. In 2016, he formed an Integrated Geomechanics Group with SRCD, and developed with his team a unique integrated fracture modeling and prediction workflow (patent pending), which is now being applied in a field's simulation prediction and history matching.

Khalid's professional interests include fracture and structural understanding and characterization using integrated geomechanics and seismic anisotropy and attributes (geometrical and elastic).

He is an active member of the Society of Exploration Geophysicists (SEG), the European Association of Geoscientists and Engineers (EAGE), and the Dhahran Geoscience Society (DGS).

Khalid received his B.S. degree in Geophysics from Tulsa University, Tulsa, OK, and his M.S. degree in Geophysics from Texas A&M University, College Station, TX. He has begun work on his Ph.D. degree with Heriot-Watt University, Edinburgh, U.K., on the azimuthal anisotropy of fractured fields.

Abdulrazaq Reda Nashar is a Geologist with Saudi Aramco's Gas Reservoir Characterization Department. He has 12 years of experience in the oil and gas industry, which includes overseas assignments in the United States, and the UAE with Baker Hughes.

Abdulrazaq's extensive experience includes well planning, geosteering, image log interpretation, supporting operations as a field geologist, work as a geologist well setter (covering Ghawar field and exploration fields), an operation geologist for the unconventional, and geomechanic geologist. His main area of focus is in geomechanical modeling and image log interpretation.

Abdulrazaq received his B.S. degree in General Geology from the University of Manchester, Manchester, U.K.

Dr. Ivan Deshenenkov is a Geologist with Saudi Aramco's Geological Operations Department. He joined Saudi Aramco in 2013 with over 10 years of petrophysical experience in both service and exploration and production companies, working in Russia, France, and the United States, specializing in petrophysics, rock physics, digital rock physics, and special core analysis.

Ivan holds several patents and has written more than 30 technical papers. He is the recipient of a grant from the Russian Presidential Grant Foundation, the Society of Petroleum Engineers (SPE) STAR Fellowship, and the American Association of Petroleum Geologists (AAPG) Gustavus E. Archie Memorial Grant for research work.

Ivan is a member of AAPG, the European Association of Geoscientists and Engineers (EAGE), and the Dhahran Geoscience Society (DGS).

In 2013, he received Ph.D. degree (with honors) in Petrophysics and Petroleum Engineering with a concentration in capillary pressures, relative permeability analysis and reservoir production forecast, from the Russian Academy of Sciences, Moscow, Russia.

Carlos A. Planchart joined Saudi Aramco in 2010 as a Geophysical Consultant working in the Geophysical Solutions Division of the Geophysical Imaging Department. His previous experience includes work as a Seismic Analyst at Western Geophysical in Caracas from 1989 to 1992. From 1993 to 2003, Carlos held several positions with Baker Hughes working in borehole seismic acquisition and processing. In 2003, he joined VSFusion as a Manager for Latin America. Then, from 2009 to 2010, Carlos worked as a Geophysical Advisor with Baker Hughes in Mexico.

In 1986, he received his B.S. degree in Physics from the Universidad de Oriente, Cumana, Venezuela, and in 1992, Carlos received his M.S. degree in Geophysics from Central University, Caracas, Venezuela.

An Effective Approach Using Microemulsion Treatment Techniques to Remove Sandstone Formation Damage: Lab Testing and Field Application

Hussain A. Almajid, Hisham I. Al-Shuwaikhat, Saleh M. Abou Zeid, and Ajay Kumar V. Addagalla

ABSTRACT

Matrix stimulation treatments executed with coiled tubing (CT) face various challenges in terms of design, execution, and evaluation. The design phase typically relies on information that is usually poorly known, e.g., extent of damage. Treatment pumping schedules and fluid concentrations are often determined based on previous experience and accepted local practices. In most cases, tools like high-pressure differential jetting nozzles are used to provide deeper penetration and lower breakout pressures. The depths at which these tools are operated usually depend on a prior log interpretation. The treatment evaluation is typically limited to the comparison of pre- and post-stimulation wellhead pressures and rates.

Over the past decade, numerous sandstone stimulation treatment alternatives have been introduced to the industry to address formation damage related issues. Yet, the same question often remains: Has the design been effectively executed and was the intervention successful?

A CT downhole measurement system, which consists of downhole gauges providing real-time data of pressure, temperature, gamma ray, and casing collar locator, has proven to be a game-changing technology with respect to treatment execution, improving both intervention efficiency and safety. The downhole measurements, along with the possibility to acquire distributed temperature surveys (DTS), have also shown to be the most effective solution for treatment evaluation to date.

This article will describe a case study of how the system can be used to optimize the acidizing treatment of damaged wells and ensure their effective stimulation. This article will also demonstrate how real-time data analysis during the intervention process can result in these intervention jobs having a high success rate.

INTRODUCTION

The following treatment design is described for two wells that were drilled and completed in the same unconsolidated sandstone formation. These wells were drilled using a synthetic oil-based mud (OBM) drilling fluid, designed to provide maximum lubrication while drilling, and minimize formation damage due to solid invasion. The wells were completed with a 9⅝" casing and a 7" liner. Due to the nature of this formation, these wells were completed with 4½" sand screens to prevent the production of the unconsolidated sand, Fig. 1. Both wells were also completed with an electric submersible pump (ESP) and Y-tool assembly as an artificial method for increased production, Fig. 2. The ESP was integrated into the Y-tool and completed as part of the tailpipe assembly to provide a means to access the wellbore.

Both wells were worked over by sidetracking them both into a different zone inside the same formation with better reservoir rock quality and pressure support. Workover operations were completed with minimal mud loss into the formation to reduce the extent of formation induced damaged. Temperature and pressure surveys were conducted for both wells after completion of workover operations, to evaluate the downhole reservoir conditions, and acquire the base distributed temperature and pressure profiles across the pay zone.

After workover operations were completed, both of these wells did not have sufficient flow and the ESP could not sustain flow, due to amperage underload. Several attempts were made to restart the ESP in these wells, but the flow rate was not able to generate enough amperage to keep the ESP running above the needed minimum amps, until eventually they were pronounced dead. A microemulsion treatment job was proposed, evaluated, and conducted to remediate these wells and improve

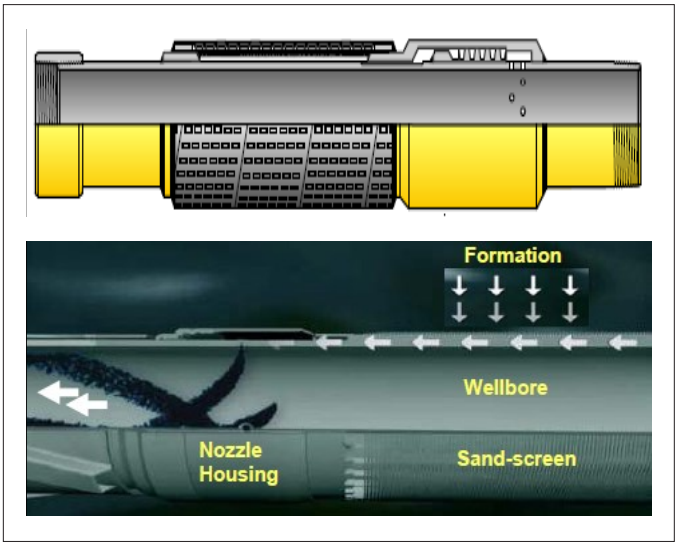

Fig. 1. A 4½" sand screen used to prevent sand production in unconsolidated sandstone reservoirs.

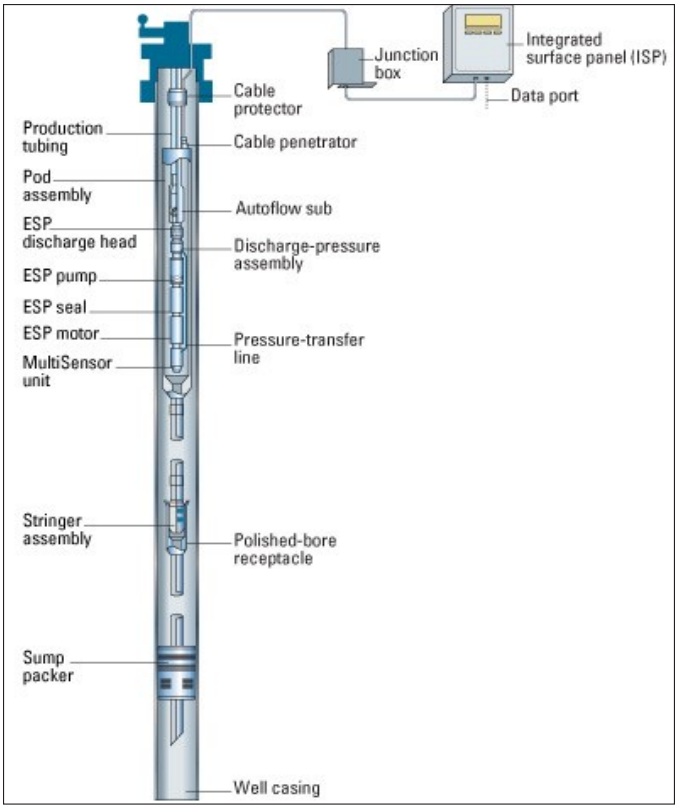

Fig. 2. Completion schematic for an ESP used as an artificial lift method.

their productivity. This article provides a new approach to maximize efficiency of the microemulsion treatment techniques in unconsolidated sandstone reservoirs.

DESCRIPTION OF TREATMENT FLUIDS

The treatment fluids for both wells included acetic acid (CH_3COOH), surfactants and corrosion inhibitors. These treatment fluids are customized to remediate and clean a reservoir with near wellbore damage and/or plugged screens, allowing the reservoir to flow at its maximum potential. The system operates by solubilizing the oil phase along with associated emulsions into a single meso-phase, to allow the acid to break the mud solids into smaller water-wet particles. After the OBM particles are broken down and dispersed, the formation fluids are able to displace these solids from the damaged zone through the wellbore until it reaches the surface. Emulsions generated from the synthetic OBM cannot be treated with a regular mud acid system of hydrochloric (HCl) acid, which is the commonly used treatment method to remediate near wellbore areas in this formation (unconsolidated sandstone).

The advantage of using microemulsion-based chemicals combined with organic acid is the ability to breakdown emulsions using surfactants, so that calcium carbonate-based bridging material can be exposed to organic acid for the chemical reaction[1, 2]. The key characteristics of this recipe is the ultralow interfacial tension and high diffusion coefficient that enables the breakdown of the emulsion layer, and creates a water-wet surface that can be easily removed by formation fluids.

GUIDELINES FOR TREATMENT DESIGN

To achieve a successful complex treatment, a set of guidelines must be considered for the candidate well to ensure the treatment will be effective in removing induced wellbore damage. The following criteria were implemented in the candidate selection for this treatment[3]:

1. Type of acid.
2. Formation mineralogy and rock properties.
3. Fluid composition.
4. Type of completion.
5. Required additives and compatibility.
6. Type of scale present based on drilling mud used.

Many of these factors, individually or in combinations, guide the selection of an appropriate formulation at which the required additives will be used for the specified job. These factors are analyzed and integrated since they dictate the treatment placement strategy. For sandstone formations, matrix stimulation strives to remove the formation damage, and therefore depends mostly on the reservoir mineralogy. Further understanding of these factors results in a direct impact in fluid penetration, optimum rate calculation, skin estimation prior to the treatment and production profile modeling post-stimulation.

FIELD APPLICATION

The treatment was implemented using 1.75” coil tubing (CT) to ensure that the treatment fluids were placed at the interface of the 4½” sand screens. The treatment application included three stages; preflush, main fluid, and overflush. The preflush fluid was used to dissolve as much of the calcareous materials as possible to minimize calcium iron precipitation, and to displace formation brines containing potassium, sodium or calcium ions

Mineral	Chemical Structure
Illite	$K_{1-1.5}Al_4[Si_{7-6.5}Al_{1-1.5}O_{20}](OH)_4$
Kaolinite	$Al_4[Si_4O_4](OH)_8$
Chlorite	$(Mg,Al,Fe)_{12}[Si,Al)_8O_{20}](OH)_{16}$
Smectite	$(½\ Ca,Na)_{0.7}(Al,Mg,Fe)_4[(Si,Al)_8O_{20}] \cdot nH_2O$

Table 1. Chemical structure for the four main types of clay minerals

Mineral	Potential Effect	Maximizes Damage	Minimizes Damage
Smectite	Swelling	Freshwater, Hydrofluoric (HF) acid	Inorganic preflush solution with low pH
Kaolinite	Mobile fines	HF	Clay stabilizer
Chlorite	Iron precipitate	High pH and O_2 rich	Iron sequester/stabilizer
Quartz, Feldspar	Mobile fines; gel precipitate	High pH	Clay stabilizer

Table 2. Sandstone minerals and their related potential effects

away from the wellbore, and to avoid forming precipitates from these minerals. The main fluid used was a mixture of acetic acid and surfactant to breakdown emulsions and disperse mud solids. Meanwhile, the overflush fluid was used to extend the reach of treatment fluid into the formation and remediate oil-wet relative permeability issues[4].

Sandstone formations contain various amounts of quartz and clays, as well as carbonates. Clay minerals are extremely small, platy-shaped materials that may be present in sedimentary rocks as packs of crystals. These clay minerals can be classified into four main groups: kaolinite group, chlorite group, illite group, and smectite group. Table 1 shows the chemical structure of the different types of clay minerals[5]. Table 2 shows the potential formation damage as a result of the interaction between the clay minerals and proposed treatment operations[4].

The types and concentrations of clay minerals present in this formation vary with depth within a single well and vary between wells within the same field. A small variation in clay percentage — 2% to 3% — can result in a drastic reduction in the formation with low porosity and tight rock properties. The main clay minerals in this formation are 0% to 40% kaolinite, 0% to 20% chlorite, 0% to 33% illite, and 0% to 73% of an ordered and random interstratified mixed layer of illite/montmorillonite.

TREATMENT IMPLEMENTATION

The case study presented in this article features two field applications in which state-of-the-art technologies were utilized to improve the efficiency of the treatment job. This technology employs the use of real-time CT downhole data to optimize fluid placement across the treatment interval based on the distributed temperature and pressure profiles. The cornerstone of this application is based on the following procedures that leverage the use of a real-time downhole data acquisition system, throughout the course of the treatment process, to optimize fluid placement using the distributed temperature and pressure profiles. A summary of this workflow is given as:

1. Run in hole up to total depth, shut-in the well, and record the baseline distributed temperature survey (DTS-1) profile.
2. Pump preflush at a constant rate below the maximum wellhead pressure with a volume calculated based on the pay zone interval, and record the DTS-2 profile.
3. Data interpretation is conducted to identify thief zones and tight zones based on the quantitive amount of flow observed during the preflush stage for low rate wells.
4. The pumping schedule is modified based on the previous step to add diverters and ensure optimal acid placement is employed.
5. Treatment is then spotted through CT while targeting the expected tight or damaged zone — referring to the open hole log. Pumps are shut-in, the well behavior is observed, and record the DTS-3 profile.
6. Finally, overflush is pumped to ensure that all treatment is squeezed inside the targeted formation zone.

EXPERIMENTAL LAB PROCEDURE

To understand the compatibility between the well itself, treatment fluids, and the formation minerals, a fluid compatibility test was conducted to analyze the byproducts resulting from the secondary and tertiary reactions. The compatibility test was conducted by adding iron carbonate ($FeCO_3$) to the same treatment fluids that were used in both wells, and monitored the reaction for any resulting byproducts. Table 3 lists the concentration and formulation for the fluids used.

A fluid compatibility test was conducted by preparing a solution of acetic acid — 10% and 15% by weight — and was formulated to match the same treatment design used in the actual treatment job. The solutions were tested by mixing them with $FeCO_3$, while varying the pH concentration for the mix from 3.0 to 5.5 with $FeCO_3$ levels of 1,000 mg/L, 3,000 mg/L, and 5,000 mg/L, Table 4. After adding $FeCO_3$, the solutions were left to stabilize at room conditions for 24 hours. For iron concentration analysis, all solutions were filtered through 0.45 micron filter paper, pipette out 1 ml of the sample and diluted

Product	Concentrations
Freshwater + Sodium Chloride	63%
Acetic Acid	10% and 15%
OHR-750	21%
OHR-AC	1.0%
OHR-759	5.0%

Table 3. The concentration and treatment fluid formulation used during the compatibility test

Iron Content	1,000 mg/L of $FeCO_3$		3,000 mg/L of $FeCO_3$		5,000 mg/L of $FeCO_3$	
Acid Used	pH	Remaining Iron in Solution (mg/L)	pH	Remaining Iron in Solution (mg/L)	pH	Remaining Iron in Solution (mg/L)
Acetic Acid 10%	3.5	975	3.7	2,589	4.0	4,560
	3.8	630	4.2	1,789	4.3	3,463
	4.1	420	4.8	530	5.2	1,752
Acetic Acid 15%	3.3	988	3.5	2,853	3.8	4,687
	3.6	832	3.7	2,367	4.1	3,456
	4.0	432	4.2	1,251	4.5	1,986

Table 4. Fluid compatibility test of $FeCO_3$ with mixtures of acetic acid at 10% and 15%

Precipitate	Origin
Iron compounds	Iron minerals or iron oxides (rust) can react with organic-HF to produce these compounds.
Calcium fluoride (CaF_2)	Carbonate-HF reaction CaF_2 can be caused by an inadequate HCl acid preflush to remove calcium ions from calcite cementing materials or to flush calcium chloride completion fluids away from the near wellbore.
Sodium and potassium fluosilicates	Feldspar and illite clay dissolution in organic acids produce these primary reaction products. They can also form if sodium or potassium brines are mixed with spent organic acids.
Aluminum hydroxides and fluorides	Clay and feldspar dissolution in HF can cause these precipitates.

Table 5. Possible precipitates during sandstone acidizing

to 100 ml. The solutions were shaken and subjected for iron analysis using inductive coupled plasma (ICP) and a Perkin-Elmer Optima 8300DV spectrometer.

LAB RESULTS AND ANALYSIS

In any treating job, the treating fluid must remove existing damage without creating additional damage through interactions with the formation rock or fluids. A formation is sensitive if the reaction between the rock minerals, and a given fluid induces damage to the formation, Table 5. The sensitivity of a formation to a given fluid includes all the detrimental reactions that can take place when this fluid contacts the rock. These detrimental reactions include the deconsolidation and collapse of the matrix, the release of fines or the formation of precipitates[6, 7].

After conducting a lab analysis on the flow back samples gathered from the treated wells, traces of solid precipitate were found. These solids were analyzed using ICP and were identified as iron ll acetate, $Fe(CH_3COO)_2$, and iron lll acetate, $Fe(CH_3COO)_3$. The purpose of this laboratory study is to identify the type of precipitates in the flow back samples, and the mechanism in which these precipitates were formed during the interaction between the treatment fluids and formation minerals.

In this compatibility test, $FeCO_3$ was mixed with an acetic acid solution — both 10% and 15% by weight — at levels of 1,000 mg/L, 3,000 mg/L, and 5,000 mg/L. Three solutions were prepared for each acetic acid group — 10% and 15%, and the pH value was modified to range from 3.0 to 5.5. After allowing the solution mix to stabilize for 24 hours at room conditions, it was evident that the amount of iron that remained in the solution decreased continuously with time as the pH value for the solution increased[8]. It is also worth noting that the 15% acetic acid solution used experienced less iron precipitation compared to the 10% acetic acid solution used, previously seen in Table 4.

In addition, none of these acids were able to re-dissolve the iron precipitate. The iron precipitate was identified as iron acetate, which is identical to the precipitate that was found in the flow back sample from the well. In addition, based on historical X-ray diffraction (XRD) data that was conducted on the treated wells, Well-A and Well-B, the abundant minerals were ankerite

Depth	Approximate Weight Percent								
	Kaolinite	Chlorite	Illite	Montmorillonite	Anhydrite	Ankerite	Siderite	Quartz	Total
8,260	1.4	3	0.9	0	Trace	5	2	87.7	100
8,265	1.7	1.2	Trace	0	0	4.8	0.5	91.8	100
8,270	0	5	0	Trace	1	6.2	3	84.8	100
8,275	1	4.6	0.8	Trace	0.5	7	Trace	86.1	100

Table 6. Formation mineral content for Well-A

Depth	Approximate Weight Percent								
	Kaolinite	Chlorite	Illite	Montmorillonite	Anhydrite	Ankerite	Siderite	Quartz	Total
5,830	0	1	0	2	4	0	1	92	100
5,835	0	1	0	2	1	Trace	0	96	100
5,840	1	Trace	Trace	1	0	2	3	93	100
5,845	0	Trace	0	0	4	2	2	92	100

Table 7. Formation mineral content for Well-B

$Ca(Mg,Fe)(CO_3)_2$ and chlorite $(Mg,Fe,Al)_6(Si,Al)_4O_{10}(OH)_8$, Tables 6 and 7, respectively. All of these minerals contain iron and are very sensitive to organic acids, which explains the high iron acetate precipitation inside the well.

$FE(CH_3COO)_2$ PRECIPITATION PROCESS

Acetic acids are monoprotic acids that dissociate, Eqn. 1; the dissociation degree of each acid is measured by its acid dissociation constant (pKa) value[9, 10]. Acids with low pKa values are stronger than the ones with higher pKa values. The pKa values also determine the distribution of ionic species; Fig. 3 shows the distribution of the ionic species of acetic acid as a function of the pH solution.

$$CH_3COOH \rightarrow CH_3COO^- + H^+,\ pKa = 4.756 \quad (1)$$

There are many sources of iron that could interact with the dissociated acetic acid (CH_3COO^-), including surface and subsurface equipment and some formation minerals like chlorite, smectite, and siderite. Therefore, the type of precipitate and conditions of precipitate formation will differ accordingly. Iron III and iron II acetate precipitates in spent acetic acid when the pH rises to around 3.8 and 4.7, respectively, according to Eqns. 2 and 3:

$$FeCO_3 + 2CH_3COOH \rightarrow Fe(CH_3COO)_2 + H_2O + CO_2$$
$$Fe^{2+} + 2(CH_3COO^-) \rightarrow Fe(CH_3COO)_2 \quad (2)$$

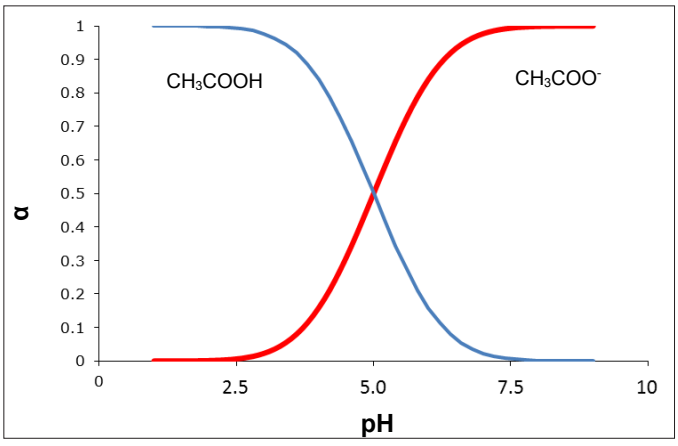

Fig. 3. The distribution of acetic acid species as a function of the pH solution value using Eqn. 1.

$$Fe_2(CO_3)_3 + 6CH_3COOH \rightarrow 2Fe(CH_3COO)_3 + 3H_2O + 3CO_2$$
$$Fe^{3+} + 3(CH_3COO^-) \rightarrow Fe(CH_3COO)_3 \quad (3)$$

An important factor that must be considered before conducting such a treatment job is the analysis of the petrophysical properties for the proposed formation. Upon further analysis of the well formation log data, it was found that this well has a nonuniform permeability profile. Once treatment fluid is pumped into these wellbore conditions, the treatment fluid will go to zones with higher permeability, leaving the low permeability areas untreated. The design of this treatment job included the use of diverters and additives to control the distribution of the treatment fluid in the formation.

POST-JOB RESULTS

Well performance evaluation showed that the proposed microemulsion treatment was effective in removing OBM filter cake and mud invaded solids, as both wells were able to sustain production at the optimum ESP design range. Previous to this treatment, both wells did not have adequate flow rates, and the ESP was tripped by amperage underload, due to the insufficient flow rates. Furthermore, pressure transient analysis conducted for these wells showed a 20% increase in the well productivity index, in comparison with the pre-job productivity index values. Lab analysis showed that minor precipitants were detected, and they were found to be mainly dependent on pH solution, acetic acid concentration, and initial mineral content.

CONCLUSIONS AND RECOMMENDATIONS

Based on post-stimulation rate gain and the fluid compatibility test conducted using the same treatment fluids, we can conclude the following:

1. The use of CT downhole gauges played a vital role in providing a qualitative and quantitative interpretation of the DTS across the treatment interval, which ultimately resulted in an optimized fluid placement across this interval.
2. The sensitivity of the formation minerology to acetic acid reaction varied from one well to another, which was mainly dependent on the type of clays and iron composition. The acetic acid (10%) used reacted with the iron (siderite) present in the formation, and $Fe(CH_3COO)_2$ precipitate

was formed, which resulted in a significant reduction in permeability.

3. The amount of $Fe(CH_3COO)_2$ precipitate was found to be mainly dependent on solution pH, acetic acid concentration, and the initial mineral content. When the solution pH value was raised, none of the tested acetic acid solutions was able to prevent $Fe(CH_3COO)_2$ precipitation.
4. Based on the fluid compatibility results for acetic acid and sandstone formation, an iron control agent is needed to prevent the precipitation of iron acetate. Iron control agents exist in two general categories: (1) iron complexing, or (2) iron sequestering agents. These additives are needed, especially at higher temperatures, where dissolved iron contents may be high. Iron control agents react with dissolved iron and other dissolved metal ions to inhibit solids precipitation, by maintaining iron cations in solution, as acid spends and the pH increases.
5. The use of spectroscopy analytical techniques, such as XRD mineralogical analysis, to determine the magnitude and potential of formation clay problems, was vital to selecting the optimal treatment fluids.
6. A clay stabilizer is often recommended for the purpose of preventing migration and/or swelling of clays following an acid treatment. Table 2 shows the various potential effects of sandstone minerals and their associated damage. Common clay stabilizers are either polyquaternary amines or polyamines, at 0.1% to 0.4%. Use of a clay stabilizer seems to be most effective when added to the overflush only.

ACKNOWLEDGMENTS

The authors would like to thank the management of Saudi Aramco and Baker Hughes, a GE company, for their support and permission to publish this article.

This article was previously presented at the SPE Kingdom of Saudi Arabia Annual Technical Symposium and Exhibition, Dammam, Saudi Arabia, April 23-26, 2018.

REFERENCES

1. Smith, C.F. and Hendrickson, A.R.: "Hydrofluoric Acid Stimulation of Sandstone Reservoirs," *Journal of Petroleum Technology*, Vol. 17, Issue 2, February 1965, pp. 215-222.
2. Abrams, A., Scheuerman, R.F., Templeton, C.C. and Richardson, E.A.: "Higher pH Acid Stimulation Systems," *Journal of Petroleum Technology*, Vol. 35, Issue 12, December 1983, pp. 2175-2184.
3. Tardy, P.M.J., Ramondenc, P., Weng, X., Burgos, R., et al.: "Inversion of Distributed-Temperature-Sensing Logs to Measure Zonal Coverage during and After Wellbore Treatment with Coiled Tubing," *SPE Productions & Operations*, Vol. 27, Issue 1, February 2012, pp. 78-86.
4. Portier, S., André, L. and Vuataz, F-D.: "Review on Chemical Stimulation Techniques in Oil Industry and Applications to Geothermal Systems," Technical Report from the Center for Geothermal Research, Neuchatel, Switzerland, May 2007, 32 p.
5. Civan, F.: *Reservoir Formation Damage: Fundamentals, Modeling, Assessment, and Mitigation*, 2nd edition, Houston, Texas: Gulf Publishing Company, 2007, 1136 p.
6. Al-Khaldi, M.H., Nasr-El-Din, H.A., Blauch, M.E. and Funkhouser, G.P.: "New Findings on Damage Potential, Geochemical Reaction Mechanisms, and Production Enhancement Applications for Citric Acid," SPE paper 82218, presented at the SPE European Formation Damage Conference, The Hague, the Netherlands, May 13-14, 2003.
7. Al-Mohammad, A.M., Al-Khaldi, M.H., Al-Mutairi, S.H. and Al-Zahrani, A.A.: "Acidizing Induced Damage in Sandstone Injector Wells: Lab Testing and a Case History," *SPE Journal*, Vol. 17, Issue 3, September 2012, pp. 885-902.
8. Al-Harbi, B.G., Al-Dahlan, M.N. and Al-Khaldi, M.H.: "Aluminum and Iron Precipitation during Sandstone Acidizing Using Organic-HF Acids," SPE paper 151781, presented at the SPE International Symposium and Exhibition on Formation Damage Control, Lafayette, Louisiana, February 15-17, 2012.
9. Crowe, C., Masmonteil, J., Touboul, E. and Thomas, R.: "Trends in Matrix Acidizing," *Oilfield Review*, Vol. 4, Issue 4, October 1992, pp. 24-40.
10. Shuchart, C.E.: "HF Acidizing Returns Analyses Provide Understanding of HF Reactions," SPE paper 30099, presented at the SPE European Formation Damage Conference, The Hague, the Netherlands, May 15-16, 1995.

BIOGRAPHIES

Hussain A. Almajid is a Production Engineer working in Saudi Aramco's Southern Area Production Engineering Department. His work experience includes work in several oil fields, including in North Ghawar and in the Southern Area. During this time, Hussain developed his experience as a skilled Production Engineer dealing with intelligent field equipment, electric submersible pumps, and smart well completions.

He has written and presented several Society of Petroleum Engineers (SPE) papers and presentations. Hussain is a certified SPE engineer.

In 2010, he received his B.S. degree in Petroleum Engineering from Louisiana State University, Baton Rouge, LA.

Hisham I. Al-Shuwaikhat is a Production Engineering Supervisor in Saudi Aramco's Khurais Production Engineering Division of the Southern Area Production Engineering Department in 'Udhailiyah. He has 12 years of oil production experience and has worked extensively in several production engineering fields within Saudi Aramco. Hisham's interest is chiefly in production engineering technology and maintaining reservoir sweep efficiency.

He is an active member of the Society of Petroleum Engineers (SPE), and has written several SPE technical and safety papers. Hisham is internationally certified in advanced root cause analysis and incident investigation by the National Examination Board in Occupational Safety (NEBOSH). Hisham is currently preparing to become a certified safety professional by the American Society of Safety Engineers (ASSE).

In 2005, he received his B.S. degree in Petroleum Engineering from King Fahd University of Petroleum and Minerals (KFUPM), Dhahran, Saudi Arabia.

Saleh M. Abo Zied is a Senior Production Engineer working in Saudi Aramco's Southern Area Production Engineering Department. He has 12 years of experience in the oil industry. Before joining Saudi Aramco, Saleh worked in the Suez Oil Company for 20 years as a Petroleum Engineering Assistant General Manager, including both in onshore and offshore oil field assignments.

He has written and presented many Society of Petroleum Engineers (SPE) papers and presentations on the subject of gas lift system optimization, devolved gas lift network, and the removal of organic deposits from oil producing wells in sandstone reservoirs.

In 1983, Saleh received his B.S. degree in Petroleum Engineering from the Faculty of Engineering, Cairo University, Sheikh Zayed City, Egypt.

Ajay Kumar V. Addagalla is currently working as the Technical Manager for Drilling and Completion at Baker Hughes, a GE company for the Saudi Arabia and Bahrain Geomarket. He has more than 9 years of oil field experience and has served in various positions in Engineering, Operations and Sales. Ajay's areas of expertise include drill-in fluids, completion fluids and near wellbore damage remediation techniques.

He received his B.Tech. degree in Chemical Engineering from Jawaharlal Nehru Technological University, Hyderabad, India, and his M.S. degree in Petroleum and Environmental Engineering from University of Nottingham, Nottingham, U.K.